Communications in Nonlinear Science and Numerical Simulation 127 (2023) 107525

Contents lists available at ScienceDirect

Communications in Nonlinear Science and Numerical Simulation

journal homepage: www.elsevier.com/locate/cnsns

Research paper

Heteroclinic chaos detecting in dissipative mechanical systems: Chaotic regimes of compound nanosatellites dynamics

Anton V. Doroshin *, Alexandr V. Eremenko

Samara National Research University Samara, Russian Federation

ARTICLE INFO

Article history:
Received 25 September 2022
Received in revised form 29 August 2023
Accepted 8 September 2023
Available online 14 September 2023

Keywords:
Heteroclinic chaos
Melnikov method adaptation
Melnikov hill
Attitude dynamics
Nanosatellite

ABSTRACT

The problem of heteroclinic chaos detecting is considered with the help of the Melnikov method. This paper presents the Melnikov method adaptation based on investigation of a nanosatellite attitude dynamics in the presence of internal dissipation properties. The need for this adaptation is determined by dynamical aspects of perturbing oscillations acting with damping amplitudes. In this case formal analytical exponential growth of perturbations values in reverse time takes place while the classical Melnikov integral does not converge.

The adaptation of the Melnikov method allows investigating the heteroclinic chaos in mechanical systems with internal dissipation properties. As a prime example of this adaptation, the research presents the complete study of chaotic attitude dynamics of a nanosatellite with a slightly movable unit under action of its damped oscillations considered as perturbations. Moreover, the considered research of the nanosatellite attitude dynamics discovers a range of important tasks in the area of a rigid body dynamics under different perturbations with damping.

Heteroclinic chaos detecting in dissipative mechanical systems: Chaotic regimes of compound nanosatellites dynamics

Anton V. Doroshin*, Alexandr V. Eremenko

Samara National Research University
Samara, Russian Federation
doran@inbox.ru*, yeryomenko.a@bk.ru

Abstract. The problem of heteroclinic chaos detecting is considered with the help of the Melnikov method. This paper presents the Melnikov method adaptation based on investigation of a nanosatellite attitude dynamics in the presence of internal dissipation properties. The need for this adaptation is determined by dynamical aspects of perturbing oscillations acting with damping amplitudes. In this case formal analytical exponential growth of perturbations values in reverse time takes place while the classical Melnikov integral does not converge.

The adaptation of the Melnikov method allows investigating the heteroclinic chaos in mechanical systems with internal dissipation properties. As a prime example of this adaptation, the research presents the complete study of chaotic attitude dynamics of a nanosatellite with a slightly movable unit under action of its damped oscillations considered as perturbations. Moreover, the considered research of the nanosatellite attitude dynamics discovers a range of important tasks in the area of a rigid body dynamics under different perturbations with damping.

1. Introduction

The analysis of homo-/heteroclinic orbits splitting and deterministic chaos parametrical study is one of the most important research topics in the dynamical systems theory. This research was developed in a continuous stream of scientific publications from the classical research of Jules Henri Poincaré to the studies of numerous more recent authors [Poincaré, H. (1899); Melnikov, V.K. (1963), Arnold V.I. (1964); Guckenheimer, J (1983); Holmes, P.J., & Marsden, J.E. (1983); Holmes, P.J. (1990); Kozlov, V.V. (1980, 1983); Lichtenberg, A.J. and Lieberman, M.A. (1983); Tabor, M. (1989); Wiggins, S. (1988-2003)].

Among the classical approaches to analyze homo-/heteroclinic chaos, we must indicate the classical Melnikov method and its generalizations. The Melnikov formalism is originating from the work of Melnikov V.K. (1963), where the homoclinic manifolds intersections were analytically detected, and the work of V.I. Arnold (1964), where this analytical technique was generalized with the help of whiskered tori theory. The multi-dimensional version of this formalism was constructed and developed by Holmes P.J. and Marsden J.E. (1983) and Wiggins S. (1988). The work of Kozlov V.V. (1980) investigated a nonintegrability of dynamical systems due to the effect of splitting homo/heteroclinic separatrices under action of perturbations; and the separatrices splitting in the rigid body dynamics was analyzed by Ziglin S.L. (1980).

Different aspects of chaotic nonlinear behavior of dynamical systems were observed in the framework of practical applications, including the tasks of space flight mechanics [Holmes, P.J. (1990); Beletskiĭ, V.V. (1995-1996); El-Gohary Awad (2005-2009); Boccaletti, S., Grebogi, C., Lai, Y. C., Mancini, H., & Maza, D. (2000); Aslanov, V.S. (2017); Chernousko, F. L., Akulenko, L. D., Leshchenko, D.D. (2017), etc.]. In practical tasks, dynamical chaos is usually considered as a negative aspect, which should be suppressed. One of the ways to suppress the chaotic behavior is the creation of dissipative forces and torques acting inside dynamical systems. Those can be generated by external dry and liquid friction, internal structural friction (in flexible mechanical systems), heat radiation, environment and medium with internal resistance, dissipative liquids flows, liquid-filled cavities, and other dynamical processes and elements [Akulenko, L. D., Kozachenko, T. A., & Leshchenko, D. D. (2019); Aslanov V.S. (2012-2021), Bao-Zeng, Y. (2011); Beletskiĭ, V.V., Pivovarov, M.L., & Starostin, E.L. (1996); Chen Li-Qun, Liu Yan-Zhu (2002); Doroshin A.V. (2012-2021); Iñarrea, M. (2009); Iñarrea, M., and Lanchares, V. (2000); Iñarrea, M., Lanchares, V., Rothos, V. M., Salas, J. P. (2003); Kuang Jinlu, Tan Soonhie, Arichandran Kandiah, Leung A.Y.T. (2001); Kuang, J.L., Meehan, P.A., Leung, A.Y.T. (2006); Liu, Y., Chen, L. (2013); Peng, J., & Liu, Y. (2000); etc.].

All of the indicated above classical works described the chaotic dynamics appearance under the action of steady oscillating perturbations with conserving amplitudes. In this regard within the framework of classical and generalized Melnikov formalisms, corresponded improper Melnikov integrals are converging.

In this work, we will consider the perturbing process as dynamical process with its own dissipation, having amplitudes of perturbing oscillations decreasing in time. This change of amplitudes is usually close to an exponential decrease to some stable levels. If we formally consider such perturbing oscillations back in time (and on the negative semiaxis of time), then we will see unbounded exponential growth of amplitudes. In this case the Melnikov integrals will be non-converging. This circumstance obviously destroys the mathematical logic of classical formalism, and the Melnikov method ceases to be workable. Therefore, it is necessary to develop some adaptation of the Melnikov method for applications with damped oscillatory perturbations. This important adaptation is presented in the section #6 of the paper.

In this paper, the adaptation of the Melnikov method is performed on the basis of task studying the attitude dynamics of a nanosatellite with small oscillations of its movable unit in the presence of constructional damping. This study represents the main applied objective of this article, but nonetheless it plays the role of a base application for the developing the fundamental approach to the extension of the Melnikov method application.

The class of micro- and nanosatellites is increasingly used in space flights and is described in scientific papers [Aslanov, V.S. (2021); Bandyopadhyay, S., Foust, R., Subramanian, G. P., Chung, S. J., & Hadaegh, F. Y. (2016); Belokonov, I. V., Timbai, I. A., & Nikolaev, P. N. (2018); Blackwell, W., Pereira, J. (2015); Doroshin, A. V. & Eremenko, A. V. (2019, 2021); Ovchinnikov, M. Y., & Roldugin, D. S. (2019); Liang He, Wenjie Ma, Pengyu Gao, Tao Sheng (2020); etc.]. Further in the paper it will be shown, that the concept of a nanosatellite with movable unit is close to the model of a rigid body with perturbations. This allows to prove the workability of presented adaptation of the Melnikov method on the basis of classical model, as well as to formulate a new range of important tasks in the framework of rigid body dynamics under different perturbations with damping.

It should be noted that the approach to estimating the Melnikov functions developed in this paper, in principle, makes it possible to obtain analytical results, but, unfortunately, we did not achieve any analytical results within the particular applied task under consideration. Therefore, in this work, numerical integration was used to estimate the specific properties of the Melnikov function.

The following assumptions were used for nanosatellite dynamics modeling. First, the attitude dynamics of a nanosatellite as a mechanical system is considered in the inertial frame, the same way as it is in the classical task of a rigid body motion about a fixed point. Moreover, we investigate the torque-free attitude dynamics of a nanosatellite, not affected by any external forces and torques. These assumptions are quite useful for modeling of the orbital dynamics on a short stretch of orbital motion. Second, all of the internal perturbations acting inside the mechanical system are small, and, therefore, we can use the linearization approach in the framework of the mathematical model construction. Third, the dissipation has natural reasons (internal friction, heat extraction, etc.), that is present inside of a mechanical system in the form of small damping perturbing oscillations.

In view of the foregoing, this article has the following structure. Section 2 presents the construction of basic models of the angular motion of a nanosatellite with the movable unit. Further, section 3 shows the reduction of a nanosatellite model to the model of a single rigid body with small perturbations based on the assumption of small oscillations of the movable unit. Section 4 provides analytical preparation to using the classical Melnikov method. Section 5 presents the analysis of dynamics with small oscillations of the movable unit having the simplest form of undamped harmonic oscillations without any dissipation, which is based on the classical Melnikov method, as well as shows the arising heteroclinic chaos. The final section 6, presents the development of the Melnikov method adaptation along with the investigation of chaotic dynamics of a nanosatellite at the presence of natural

dissipation with damping of perturbing oscillations with the help of the mentioned adapted method.

2. Mechanical and mathematical models

Let us consider the mechanical model (fig.1) of a nanosatellite with a movable unit [Doroshin, A. V., & Eremenko, A. V. (2019, 2021)]. In this case, the nanosatellite consists of two parts - the carrying main body, and the movable unit, attached to the carrier body by means of flexible rods.

The movable unit can perform angular motion relative to the main body due to changing the lengths of the flexible rods. We shall assume that the point O is the rotation center of the movable unit, i.e. the point O is fixed relative to the main body.

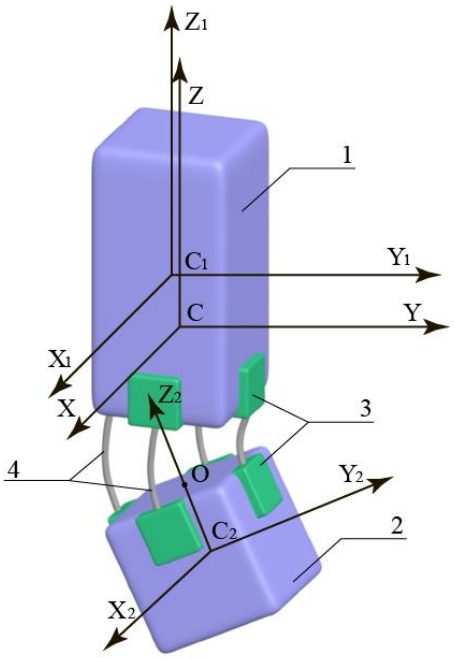

Figure 1 – The nanosatellite structure:
1 – the main body, 2 – the movable unit, 3 – control systems of flexible rods extraction, 4 – flexible rods.

In the present research we will use the following coordinate systems:

- $C_1X_1Y_1Z_1$ is a principal body-fixed coordinate frame of the main body, where the point C_1 is the center of mass of the main body;

- $C_2X_2Y_2Z_2$ is a principal body-fixed coordinate frame of the movable unit, where the point C_2 is the center of mass of the movable unit;

- CXYZ is a coordinate frame with the origin in the center of mass of the complete system, which axes are parallel to the main axes of the main body. The point C is the center of mass of the complete nanosatellite.

Let us write the expression for the system angular momentum as the sum of the angular momentums of its parts. The angular momentum vector in the coordinate frame $CXYZ$ has the form:

$$\mathbf{K} = \mathbf{K_1} + \boldsymbol{\delta}_\mathbf{1}\mathbf{K_2}, \tag{1}$$

where $\boldsymbol{\delta}_\mathbf{1}$ is the transition matrix from the $C_2X_2Y_2Z_2$ coordinate system to the $C_1X_1Y_1Z_1$ coordinate system, $\mathbf{K_1}$ – is the angular momentum of the main body in the frame $C_1X_1Y_1Z_1$, $\mathbf{K_2}$ – is the angular momentum of the movable unit in projections on axes $C_2X_2Y_2Z_2$.

Let us assume that the angular displacements of the movable unit can be possible only around the direction C_2X_2 on a small angle $\alpha << 1$. Then the following linearized matrix takes place (we neglect the terms of order α^2 or less):

$$\boldsymbol{\delta}_\mathbf{1} = \begin{bmatrix} 1 & 0 & 0 \\ 0 & 1 & -\alpha \\ 0 & \alpha & 1 \end{bmatrix}. \tag{2}$$

The angular momentums of the nanosatellite parts in CXYZ are:

$$\mathbf{K_1} = \mathbf{I_1}\boldsymbol{\omega}_\mathbf{1}, \tag{3}$$

$$\mathbf{K}_2 = \mathbf{I}_2\boldsymbol{\omega}_2, \tag{4}$$

where $\mathbf{I}_1, \mathbf{I}_2$ – are the inertia tensors of the main body and the movable unit:

$$\mathbf{I}_1 = \begin{bmatrix} I_{1x} & 0 & 0 \\ 0 & I_{1y} & \alpha k_1 \\ 0 & \alpha k_1 & I_{1z} \end{bmatrix}, \tag{5}$$

$$\mathbf{I}_2 = \begin{bmatrix} I_{2x} & 0 & 0 \\ 0 & I_{2y} & \alpha k_2 \\ 0 & \alpha k_2 & I_{2z} \end{bmatrix}, \tag{6}$$

m_1 is the mass of the carrier body, m_2 – is the mass of the movable unit, $k_1 = -m_1 l_2 (l_1 - z_1 - l_2)$, $k_2 = -m_2 l_1 (l_1 + z_2 - l_2)$, $l_1 = m_1 z_1 / (m_2 + m_2)$, $l_2 = m_2 z_2 / (m_2 + m_2)$, z_1 – is the distance between points C_1 and O, z_2 – is the distance between points C_2 and O. For the moments of inertia, we have the following expressions obtained with the help of the Steiner's theorem while neglecting the terms of the second order by a small angle $(\alpha^2 \to 0)$ or less:

$$I_{1x} = A_b + m_1 (z_1 - l_1 + l_2)^2;\ I_{1y} = B_b + m_1 (z_1 - l_1 + l_2)^2;\ I_{1z} = C_b;$$

$$I_{2x} = I_{2y} = A_u + m_2 (l_2 - z_2 - l_1)^2;\quad I_{2z} = C_u,$$

where (A_b, B_b, C_b) – are the main central moments of inertia of the main body and (A_u, B_u, C_u) – are the main central moments of inertia of the movable unit (the unit is dynamically symmetrical and, therefore, B_u=A_u).

The angular velocity of the main body in projections on the axes of the $C_1X_1Y_1Z_1$ coordinate system is:

$$\boldsymbol{\omega_1} = \left[p, q, r \right]^T . \tag{7}$$

Taking into account the relative rotation, the angular velocity of the movable unit in projections on the axes of the $C_2X_2Y_2Z_2$ is:

$$\boldsymbol{\omega_2} = \boldsymbol{\delta_2} \begin{bmatrix} p \\ q \\ r \end{bmatrix} + \begin{bmatrix} \dot{\alpha} \\ 0 \\ 0 \end{bmatrix} = \begin{bmatrix} p + \dot{\alpha} \\ q + \alpha r \\ r - \alpha q \end{bmatrix}, \tag{8}$$

where $\boldsymbol{\delta_2}$ – is the linearized transition matrix from the coordinate system $C_1X_1Y_1Z_1$ to the $C_2X_2Y_2Z_2$:

$$\boldsymbol{\delta_2} = \begin{bmatrix} 1 & 0 & 0 \\ 0 & 1 & \alpha \\ 0 & -\alpha & 1 \end{bmatrix}. \tag{9}$$

To analyze the attitude dynamics of the nanosatellite, it is appropriate to write dynamical equations using the well-known canonical Serret-Andoyer-Deprit variables [Andoyer H. (1923), Deprit A. (1967), Serret, J. A. (1866)]. The Serret-Andoyer-Deprit variables (h, g, l) and corresponding canonical conjugate momenta (H, G, L) describing the spatial position of the angular momentum vector **K** relatively the main coordinates frame CXYZ and the "fixed inertial" frame Cξηζ. Here it is appropriate to give a brief description of the canonical Serret-Andoyer-Deprit variables. Let us build a plane CBE orthogonal to the angular momentum vector **K**. This plane intersects the plane Cξη along the straight line CB, and also intersects the plane CXY along the straight line CE. Then the planar arc AB corresponds to the angle h; the planar arc BE corresponds to the angle g; the planar arc EF corresponds to the angle l. The corresponding canonical conjugate momenta are denoted as H, G, L. Moreover, it is known that G=|**K**|, H=**K**·**k'**, L=**K**·**k**, where **k** and **k'** are the unit-vectors of axes CZ and Cζ.

The angular momentum components in the frame CXYZ can be expressed through the Serret-Andoyer-Deprit variables in the form:

$$\begin{cases} K_x = \sqrt{G^2 - L^2}\sin l; \\ K_y = \sqrt{G^2 - L^2}\cos l; \\ K_z = L. \end{cases} \tag{10}$$

In addition, we must add the canonical momentum A for the relative rotation

angle α:

$$\mathrm{A} = \frac{\partial T}{\partial \dot{\alpha}} = I_{2x}\left(p + \dot{\alpha}\right), \tag{11}$$

where T is the kinetic energy of the nanosatellite:

$$T = \frac{1}{2}\left(\mathbf{K_1} \cdot \boldsymbol{\omega_1} + \mathbf{K_2} \cdot \boldsymbol{\omega_2}\right). \tag{12}$$

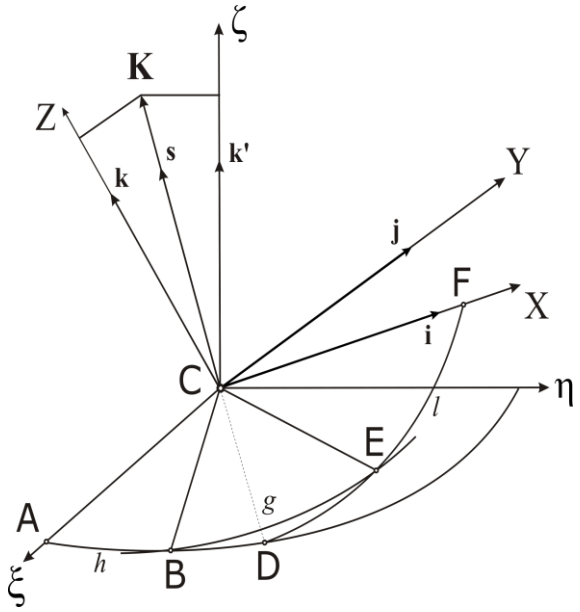

Figure 2 – The canonical Serret-Andoyer-Deprit variables

Using (7)-(12) we can explicitly express $p, q, r, \dot{\alpha}$ in terms of the Serret-Andoyer-Deprit variables:

$$\begin{cases} \widehat{p} = \dfrac{\mathrm{A} - \sqrt{G^2 - L^2}\sin l}{I_{2x} - I_{cx}}; \\ \widehat{q} = \dfrac{I_{cz}\sqrt{G^2 - L^2}\cos l - \alpha k L}{I_{cy} I_{cz}}; \\ \widehat{r} = \dfrac{I_{cy} L - \alpha k \sqrt{G^2 - L^2}\cos l}{I_{cy} I_{cz}}; \\ \widehat{\dot{\alpha}} = \dfrac{I_{2x}\sqrt{G^2 - L^2}\sin l - I_{cx}\mathrm{A}}{I_{2x}\left(I_{2x} - I_{cx}\right)}; \end{cases} \tag{13}$$

where $I_{cx} = I_{1x} + I_{2x}$, $I_{cy} = I_{1y} + I_{2y}$, $I_{cz} = I_{1z} + I_{2z}$, $k = I_{2y} + k_2 + k_1 - I_{2z}$, and where terms of order higher than one in α have been neglected. The symbol "$\widehat{\ }$" above the variable now and further indicates the explicit expressions for angular velocity components through the Serret-Andoyer-Deprit canonical variables – these expressions will be substituted into the expression of the kinetic energy to write the

explicit expression of the Hamiltonian. On the basis of equations (12) and (13) we can write the explicit Hamiltonian of the mechanical system in potential fields:

$$\mathcal{H}\left(\hat{p},\hat{q},\hat{r},\hat{\dot{\alpha}},\alpha\right)=T\left(l,g,h,\alpha,L,G,H,\mathrm{A}\right)+P\left(l,g,h,\alpha\right). \tag{14}$$

3. The general case of the system motion close to rigid body dynamics

At the start of our research, we will consider the torque-free dynamics of considered system in a "monobody" format without any external and internal forces. This will be the general unperturbed case, when we investigate the torque-free motion of the nanosatellite as a mechanical system consisting from two rigid bodies "glued into a single rigid form" (at small relative angular displacement of the movable unit). Due to the smallness of the angle α of a relative position of the movable unit, the described mechanical system can be considered as a rigid body, but in the presence of small changes of its inertia-geometrical parameters depending on the α value [Doroshin, A. V., & Eryomenko, A. V. (2021-b)]. Then we can consider the angle α as a geometrical parameter, which defines the geometrical/kinematical constrain $\alpha = \alpha(t)$. This assumption allows to write the general unperturbed expression for the Hamiltonian as the Hamiltonian of the torques-free single rigid body with small parametrical perturbations:

$$\mathcal{H}=T. \tag{15}$$

In this consideration, the fourth canonical coordinate and corresponding canonical momentum $\{\alpha, \mathrm{A}\}$ lose their independent meaning. Then it is possible to write the following expressions for $\{p, q, r\}$ through the Serret-Andoyer-Deprit canonical coordinates formally introduced for a single rigid body with small additions:

$$\begin{cases} \hat{p}=\hat{p}_0-\dfrac{I_{2x}}{I_{cx}}\dot{\alpha}; \\ \hat{q}=\hat{q}_0-\dfrac{\alpha k\hat{r}_0}{I_{cy}}; \\ \hat{r}=\hat{r}_0-\dfrac{\alpha k\hat{q}_0}{I_{cz}}; \end{cases} \tag{16}$$

where the following expressions are completely correspond to the Serret-Andoyer-Deprit coordinates for a single rigid body with general inertia tensor $\hat{\mathbf{I}}=diag\left(I_{cx},I_{cy},I_{cz}\right)$:

$$\begin{cases} \hat{p}_0=\dfrac{1}{I_{cx}}\sqrt{G^2-L^2}\sin l; \\ \hat{q}_0=\dfrac{1}{I_{cy}}\sqrt{G^2-L^2}\cos l; \\ \hat{r}_0=\dfrac{L}{I_{cz}}. \end{cases} \tag{17}$$

Substituting equation (16) into (12), we will obtain the expression of the kinetic energy and the Hamiltonian at the linear approximation by α:

$$\mathcal{H} = \frac{1}{2}\left(I_{cx}\hat{p}_0^{\,2} + I_{cy}\hat{q}_0^{\,2} + I_{cz}\hat{r}_0^{\,2} \right) - k\alpha\hat{q}_0\hat{r}_0 + \frac{I_{1x}I_{2x}}{2I_{cx}}\dot{\alpha}^2 . \qquad (18)$$

It is possible to divide the expressions (18) in parts, proportional to a small parameter μ. Then we will have a "generating part" $\mathcal{H}_0$ and perturbed parts $\mu\mathcal{H}_1$, $\mu^2\mathcal{H}_2$:

$$\mathcal{H} = \mathcal{H}_0 + \mu\mathcal{H}_1 + \mu^2\mathcal{H}_2 + \ldots , \qquad (19)$$

where

$$\mathcal{H}_0 = \frac{1}{2}\left(I_{cx}\hat{p}_0^{\,2} + I_{cy}\hat{q}_0^{\,2} + I_{cz}\hat{r}_0^{\,2} \right) = \frac{1}{2}\left[\left(G^2 - L^2 \right)\left(\frac{\sin^2 l}{I_{cx}^2} + \frac{\cos^2 l}{I_{cy}^2} \right) + \frac{L^2}{I_{cz}^2} \right], \qquad (20)$$

$$\mu\mathcal{H}_1 = -\mu\tilde{\alpha}k\hat{q}_0\hat{r}_0 = -\mu\tilde{\alpha}k\frac{L}{I_{cy}I_{cz}}\sqrt{G^2 - L^2}\cos l , \qquad (21)$$

$$\mu^2\mathcal{H}_2 = \mu^2\frac{I_{1x}I_{2x}}{2I_{cx}}\dot{\tilde{\alpha}}^2 . \qquad (22)$$

Here μ is a formal small dimensionless parameter $(\mu << 1)$ denoting the small deviation of relative angular motion of the movable unit $\alpha = \mu\tilde{\alpha}$. It is worth to note, that the part (22) formally follows from the kinetic energy expression (18) as the term proportional to the second power of the small parameter, but this part will be real small at a smallness assumption of the angular velocity $\dot{\alpha}$. On the other hand, the part (22) do not contain any Serret-Andoyer-Deprit coordinates, and, therefore, it will not influence on dynamics of the considered dynamical system in the Serret-Andoyer-Deprit phase space. In any case, we shall omit the term $\mu^2\mathcal{H}_2$ from the following research.

So, the expression (19) corresponds to the usual Hamiltonian of the unperturbed rigid body $\mathcal{H}_0$ with small perturbations proportional to the first power of the small parameter $(\mu\mathcal{H}_1)$ defined by variability of the "geometrical" parameter α. Then the system of Hamilton's equations in the Serret-Andoyer-Deprit canonical coordinates is:

$$\begin{aligned} \dot{L} &= -\frac{\partial\mathcal{H}}{\partial l}; \quad & \dot{l} &= \frac{\partial\mathcal{H}}{\partial L}; \\ \dot{H} &= -\frac{\partial\mathcal{H}}{\partial h}; \quad & \dot{h} &= \frac{\partial\mathcal{H}}{\partial H}; \\ \dot{G} &= -\frac{\partial\mathcal{H}}{\partial g}; \quad & \dot{g} &= \frac{\partial\mathcal{H}}{\partial G}. \end{aligned} \qquad (23)$$

As we can see from the Hamiltonian (19)-(21), the mechanical system is completely described by the pare of coordinates (l, L), since

$$\dot{H} = -\frac{\partial\mathcal{H}}{\partial h} = 0 , \quad \dot{h} = \frac{\partial\mathcal{H}}{\partial H} = 0 , \quad \dot{G} = -\frac{\partial\mathcal{H}}{\partial g} = 0 .$$

The coordinate $g(t)$ can be integrated separately after the integrations for (l, L), and,

therefore, the coordinate $g(t)$ do not influence on the main dynamical properties.

For convenience, we write the system of differential equations (23) in the following form:

$$\dot{L} = f_L + \mu g_L; \quad \dot{l} = f_l + \mu g_l; \tag{24}$$

where

$$\begin{aligned} f_L &= -\frac{\partial \mathcal{H}_0}{\partial l}; \;\; g_L = -\frac{\partial \mathcal{H}_1}{\partial l}; \\ f_l &= \frac{\partial \mathcal{H}_0}{\partial L}; \quad\; g_l = \frac{\partial \mathcal{H}_1}{\partial L}. \end{aligned} \tag{25}$$

The system (24) completely describes the dynamics of a rigid body in the presence of small perturbations in its inertia parameters due to small variability of the body shape (in accordance with the "geometric" parameter α) in the linear approximation.

4. Detecting the possibility of chaotic regimes in dynamics

It is a known fact, that a rigid body under the action of external perturbations or in the presence of internal asymmetric rotators or movable elements can have chaotic regimes of the angular motion [Aslanov, V.S. & Doroshin, A.V. (2010), Aslanov, V. S. (2015), Aslanov, V.S. (2021), Beletsky V.V. (1995), Chen Li-Qun, Liu Yan-Zhu (2002), Doroshin, A.V. (2012-2018), Doroshin, A. V., & Eremenko, A. V. (2019, 2021-b), Holmes, P.J., & Marsden, J.E. (1983), Iñarrea, M. (2009), Iñarrea, M. & Lanchares, V. (2000), Iñarrea, M., Lanchares, V., Rothos, V. M., Salas, J. P. (2003), Kuang Jinlu, Tan Soonhie, Arichandran Kandiah, Leung A.Y.T. (2001), Kuang, J.L., Meehan, P.A., Leung, A.Y.T. (2006), Leung, A.Y.T., Kuang, J.L. (2007), Peng, J., & Liu, Y. (2000), Ziglin S. L. (1980)].

The chaotic dynamics can be associated with the presence of homo/heteroclinic nets in the system phase space. To detect the homo/heteroclinic nets we can use the Melnikov's method [Melnikov, V.K. (1963)] and its multidimensional modifications of Wiggins [Wiggins, S. (1988-2003)] or Holmes and Marsden [Holmes, P.J., & Marsden, J.E. (1983)].

In this section of the article, we will use the classical Melnikov method. In accordance with this method, the fact of the appearance of chaos can be confirmed by the presence of simple roots of the so-called Melnikov function.

The Melnikov function for the perturbed system (24) has the form:

$$M(t_0) = \int\limits_{-\infty}^{+\infty} \{\mathcal{H}_0, \mathcal{H}_1\}\Big|_{\left(\bar{L}(t),\bar{l}(t),t+t_0\right)} dt = \int\limits_{-\infty}^{+\infty} \left[\, f_L g_l - f_l g_L \,\right]\Big|_{\left(\bar{L}(t),\bar{l}(t),t+t_0\right)} dt\,, \tag{26}$$

where $\{\cdot,\cdot\}$ is the Poisson bracket. Here $\bar{L}(t), \bar{l}(t)$ are the explicit exact solutions corresponding to one of the four possible heteroclinic orbits, which can be expressed through the well-known heteroclinic solutions $\left(\bar{p}_0(t), \bar{q}_0(t), \bar{r}_0(t)\right)$ for the torque-free dynamics of a rigid body [Holmes, P.J., & Marsden, J.E. (1983); Iñarrea, M., Lanchares, V., Rothos, V. M., Salas, J. P. (2003); etc.]:

$$\begin{cases} \overline{p}_0(t) = \dfrac{(-1)^{\mathrm{int}(j/2)}}{\mathrm{ch}(at)} \sqrt{\dfrac{T_0\left(I_{cy}-I_{cz}\right)}{I_{cx}\left(I_{cx}-I_{cz}\right)}}; \\ \overline{q}_0(t) = (-1)^j \,\mathrm{th}(at) \sqrt{\dfrac{T_0}{I_{cy}}}; \\ \overline{r}_0(t) = \dfrac{(-1)^{\mathrm{int}((j-1)/2)}}{\mathrm{ch}(at)} \sqrt{\dfrac{T_0\left(I_{cx}-I_{cy}\right)}{I_{cz}\left(I_{cx}-I_{cz}\right)}}; \end{cases} \tag{27}$$

where the number $j = [1,2,3,4]$ selects one of the four heteroclinic trajectories; the operation $\mathrm{int}(x)$ denotes the integer part of the number x; $a = \sqrt{T_0\left(I_{cx}-I_{cy}\right)\left(I_{cy}-I_{cz}\right)/\left(I_{cx}I_{cy}I_{cz}\right)}$; T_0 - is the initial value of the doubled kinetic energy E of the rigid body on the heteroclinic trajectory:

$$T_0 = 2E = \mathrm{const}, \tag{28}$$

where

$$E = \frac{1}{2}\left(I_{cx}\overline{p}_0^2 + I_{cy}\overline{q}_0^2 + I_{cz}\overline{r}_0^2\right).$$

In solutions (27) and further in the paper the following restriction for inertia moments is actual:

$$I_{cx} > I_{cy} > I_{cz}.$$

Now we need to write the functions f_L, f_l, g_L, g_l. With the help of the expressions (17) it is possible to obtain:

$$\begin{aligned} & f_l\left(\overline{L}(t),\overline{l}(t)\right) = \overline{r}_0 - I_{cz}\overline{r}_0(t)\frac{\overline{p}_0^2(t)I_{cx} + \overline{q}_0^2(t)I_{cy}}{G^2 - \overline{r}_0^2(t)I_{cz}^2}; \\ & f_L\left(\overline{L}(t),\overline{l}(t)\right) = \left(I_{cx}-I_{cy}\right)\overline{p}_0(t)\overline{q}_0(t); \\ & g_l\left(\overline{L}(t),\overline{l}(t),t+t_0\right) = k\left(\frac{\overline{q}_0(t)\overline{r}_0^2(t)I_{cz}}{G^2 - \overline{r}_0^2 I_{cz}^2} - \frac{\overline{q}_0(t)}{I_{cz}}\right)\tilde{\alpha}(t+t_0); \\ & g_L\left(\overline{L}(t),\overline{l}(t),t+t_0\right) = -\frac{kI_{cx}}{I_{cy}}\overline{p}_0(t)\overline{r}_0(t)\tilde{\alpha}(t+t_0). \end{aligned} \tag{29}$$

Then the integrand in (26) has the following form:

$$\left[f_L g_l - f_l g_L\right]\Big|_{\left(\overline{L}(t),\overline{l}(t),t+t_0\right)} = \tilde{\alpha}(t+t_0)\, f\left(\overline{p}_0(t),\overline{q}_0(t),\overline{r}_0(t)\right), \tag{30}$$

where

$$f(t)=f\left(\bar{p}_0(t),\bar{q}_0(t),\bar{r}_0(t)\right)=k\bar{p}_0\left(\bar{q}_0^2\frac{I_{cx}-I_{cy}}{I_{cz}}\left(\frac{\bar{r}_0^2I_{cz}^2}{G^2-\bar{r}_0^2I_{cz}^2}-1\right)+\right.$$
$$\left.+\bar{r}_0^2\frac{I_{cx}}{I_{cy}}\left(1-I_{cz}\frac{\bar{p}_0^2I_{cx}+\bar{q}_0^2I_{cy}}{G^2-\bar{r}_0^2I_{cz}^2}\right)\right). \quad (31)$$

Taking into account the fact, that the component $\bar{p}_0(t)$ is an even function (this follows from (27)), and that $\bar{p}_0^2$, $\bar{q}_0^2$, $\bar{r}_0^2$ are also even functions, we can conclude that the function *f*(*t*), given in (31), is also an even function (fig.3).

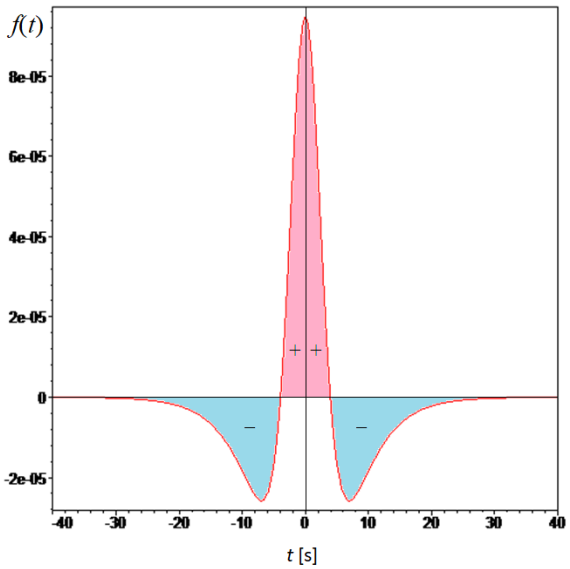

Figure 3 – The typical form of the function *f*(*t*) (31)

Now to detect chaotic regimes using the Melnikov's function (26) we only need to know the specific functional form of dependence $\alpha=\alpha(t+t_0)$, which defines the result of the improper integration (30).

5. The analysis of the chaotic dynamics on the assumption of simplest perturbation forms

As a first simplest but a very important case of dynamical analysis, in this section we will use the time-dependence of the angle $\alpha = \alpha(t)$, which corresponds to the simplest harmonic form:

$$\begin{aligned} &\alpha = \mu\tilde{\alpha} = \mu\cos(\Omega t + \Omega t_0); \\ &\Omega = \text{const}; \quad \mu << 1. \end{aligned} \tag{32}$$

The form (32), foremost, can simulate usual simplest flexible oscillations of the movable unit on flexible elastic rods neglecting the factor of dissipation properties (this can be an appropriate simulation at least for some finite time interval). Secondly, the small harmonic oscillations (32) can arise due to small error-delays in the control system [Doroshin, A. V., & Eremenko, A. V. (2021-a)], stabilizing the relative longitudinal angular position of the movable unit. In addition, such oscillations can be intentionally generated by the control system to ensure the transition to the chaotic mode [Doroshin, A. V. (2018-b)] for the purpose of nanosatellite reorientation. In any case, the form (32) can be used as a simplest primary perturbing factor to the direct application of the classical Melnikov method.

The substitution of the expression (32) into (30) after simplifications gives the following Melnikov function:

$$M(t_0) = \mu\cos(\Omega t_0)\int_{-\infty}^{+\infty}\cos(\Omega t)\,f(t)dt - \mu\sin(\Omega t_0)\int_{-\infty}^{+\infty}\sin(\Omega t)\,f(t)dt\,. \tag{33}$$

As it was already indicated above, the function $f(t)$ is an even function. Since $\sin(t)$ is an odd function, the improper integral of the odd function $f(t)\sin(t)$ will be equal to zero, and, therefore:

$$M(t_0) = \mu\cos(\Omega t_0)\int_{-\infty}^{+\infty}\cos(\Omega t)\,f(t)\,dt\,. \tag{34}$$

The integrand in (34) is an even function, and then the value of the improper integral will correspond to the nonzero signed area Λ bounded by $\cos(\Omega t)\,f(t)$:

$$M(t_0) = \mu\cos(\Omega t_0)\int_{-\infty}^{+\infty}\cos(\Omega t)\,f(t)\,dt = \mu\Lambda\cos(\Omega t_0), \tag{35}$$

$$\Lambda = \int_{-\infty}^{\infty} f(t)\cos(\Omega t)dt = \text{const} \neq 0\,. \tag{36}$$

As we can see, the Melnikov function in the considered simplest case is the function (35) with usual oscillatory behavior and with nonzero amplitude (36). The amplitude (36) will be equal to zero only in critical cases when Ω=0 and Ω=∞, that can be checked numerically (fig.4-a). Therefore, the Melnikov function has infinite quantity of simple roots. This fact proves the presence of the heteroclinic chaos in the dynamics. To illustrate the corresponded heteroclinic chaos in this case we can plot the Poincaré section/map for unperturbed (fig.4-b) and perturbed (fig.4-c..f) dynamics at some nonzero values of the parameters μ and Ω.

All of the calculations here and in other sections of this article were performed using the numerical values of parameters from the table 1.

The Poincaré sections (fig.4–b..f) represent complete forms of the main phase space (l, L/G) in dynamical sense and fully describe the dynamical behavior for all of the possible initial values. Points of the Poincaré section are added on the plane (l, L/G) at fulfilling of predefined conditions. Within the present research the "stroboscopic" condition is selected, and the points are added to the Poincaré section at discrete time-moments when $\mathrm{mod}\left(t, 2\pi/\Omega\right) = 0$.

As it is known, the points of the Poincaré sections can form continuous lines, corresponding to the regular phase trajectories, or vice versa, can fill by individual points entire regions of the phase plane – they can be called as the "chaotic layers".

Table 1 – Inertia-mass parameters of the nanosatellite
and initial conditions of the motion along the heteroclinic trajectory

Parameters	**Values**	**Parameters**	**Values**
m_1 [kg]	2	m_2 [kg]	1
A_b [kg·m^2]	0.013	A_u [kg·m^2]	0.0025
B_b [kg·m^2]	0.009	B_u [kg·m^2]	0.0025
C_b [kg·m^2]	0.006	C_u [kg·m^2]	0.0035
z_1 [m]	0.08	z_2 [m]	0.04
χ [kg·m^2/s^2]	0.006	T_0 [kg·m^2/s^2]	0.0054
$\alpha(0)$ [rad]	0.1	$\overline{p}_0(0)$ [rad/s]	0.4000
$\dot{\alpha}(0)$ [rad/s]	0	$\overline{q}_0(0)$ [rad/s]	0.0000
G [kg·m^2/s]	0.0107	$\overline{r}_0(0)$ [rad/s]	-0.3818

As we can see, in the absence of perturbations the considered system has the quality form of the physical pendulum (fig.4-b). We can notice the chaotic layers to appear under the perturbations (fig.4-c..f), as well as the generation of new additional heteroclinic bundles of secondary separatrices, which can also be splatted under perturbations.

The Poincaré sections (fig.4) can quite fully explain the main dynamical properties of the attitude motion of the nanosatellite. The same technique of the "stroboscopic" Poincaré sections will be used below in studying cases of the system dynamics at the perturbing oscillations with damping. In addition the fig.4 also demonstrates the influence of the perturbation frequency Ω on the width of chaotic layers in accordance with the frequency response Λ(Ω) (fig.4-a).

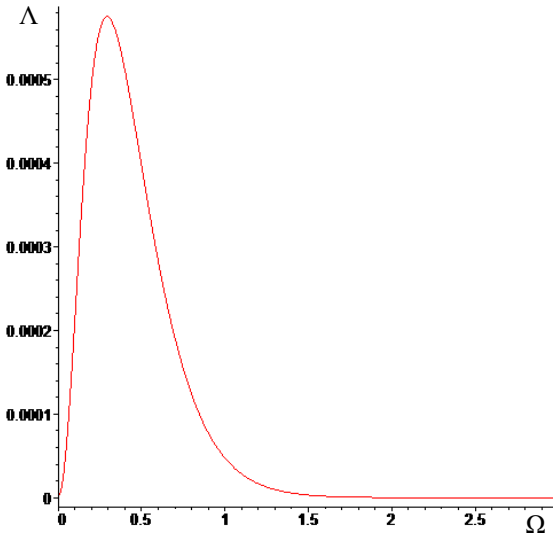

(a): the amplitude (36)

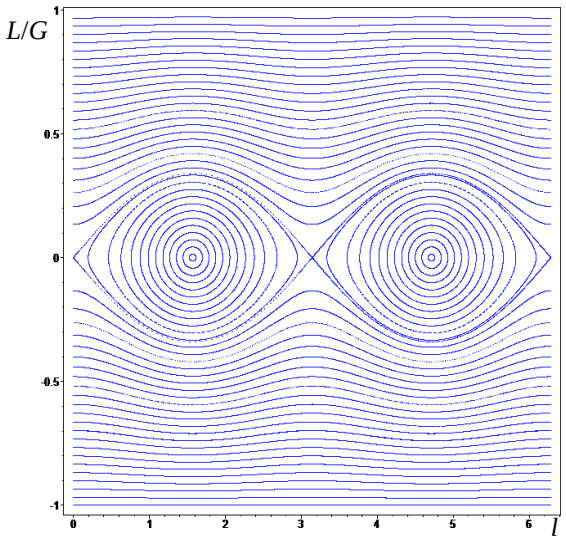

(b): μ=0.0; Ω=1.0 (∀Ω)

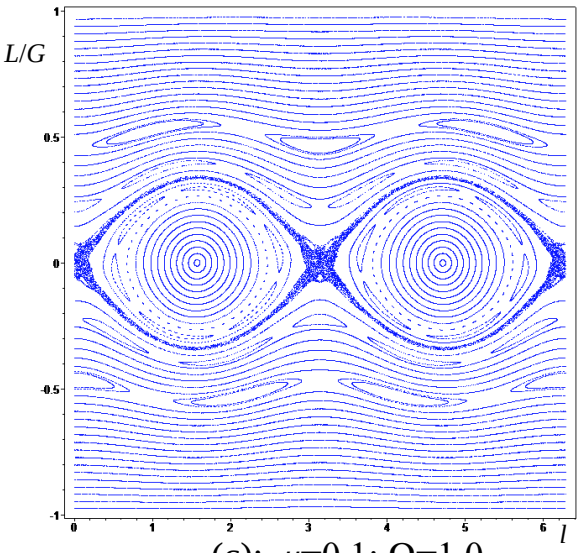

(c): μ=0.1; Ω=1.0

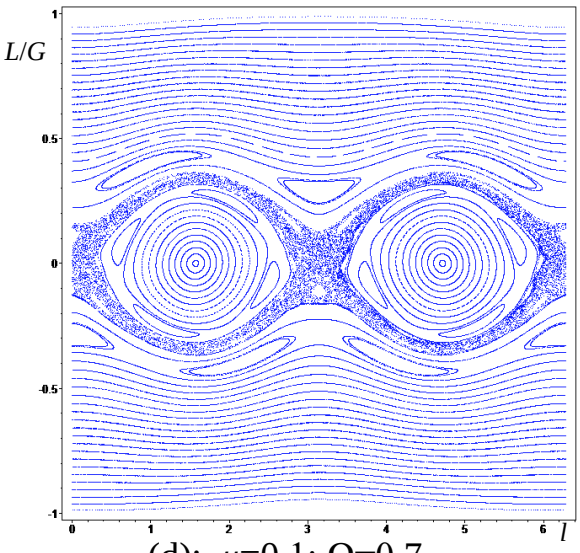

(d): μ=0.1; Ω=0.7

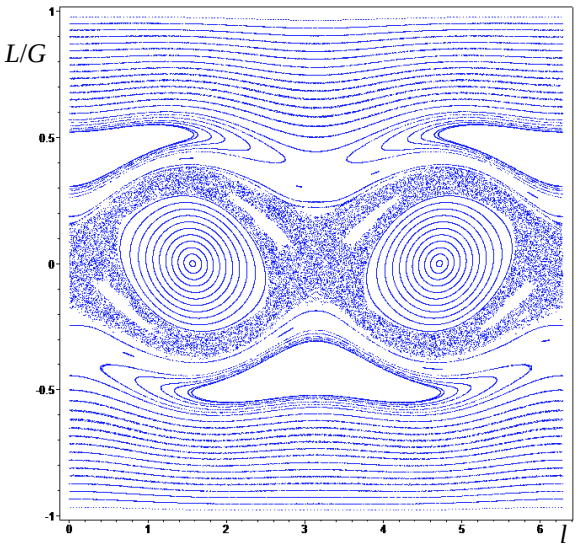

(e): μ=0.1; Ω=0.3

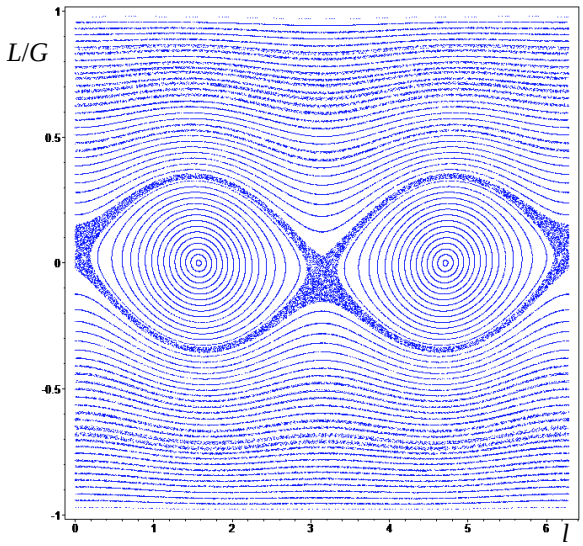

(f): μ=0.1; Ω=0.1

Figure 4 – The amplitude Λ(Ω) and Poincaré sections

6. The chaos detection in the dynamics of a dissipative system with damping natural perturbations

6.1. The solution for perturbing oscillations

Now let us consider the case of the nanosatellite motion when disturbances caused by the natural dynamics. To obtain the natural form of the small perturbation $\alpha(t)$, we can use the Lagrange formalism, which allows to write the equation:

$$\frac{d}{dt}\left(\frac{\partial T}{\partial \dot{\alpha}}\right)-\frac{\partial T}{\partial \alpha}=M_{\alpha}. \tag{37}$$

The torque M_{α} is caused by the elastic forces of the flexible rods, and by the friction forces:

$$M_{\alpha}=-\nu\dot{\alpha}-\chi\alpha. \tag{38}$$

where $\nu\ \left[\mathrm{kg}\times \mathrm{m}^2/\mathrm{s}\right]$, $\chi\ \left[\mathrm{kg}\times \mathrm{m}^2/\mathrm{s}^2\right]$ – are coefficients of damping and elasticity, which also can be considered as feedback coefficients of the control system to extracting the flexible rods and to rotating the movable unit (fig.1).

From expressions (38) and (37) we can obtain the equation:

$$\ddot{\alpha}=-\left(k\hat{q}_0\hat{r}_0+\nu\dot{\alpha}+\chi\alpha\right)\frac{I_{cx}}{I_{2x}I_{1x}}. \tag{39}$$

If we substitute into (39) the dependencies for the heteroclinic trajectory, then we can describe the dynamics of the angle α strictly along the heteroclinic separatrix (27). It is the dynamics of $\alpha(t)$ in the vicinity of the separatrix, which we will consider as the perturbing dynamics. In this case, we can write the equation:

$$\dot{\boldsymbol{\varphi}}=\mathbf{M}\cdot\boldsymbol{\varphi}+\mathbf{F}\left(t\right), \tag{40}$$

where

$$\begin{gathered}\boldsymbol{\varphi}=\begin{bmatrix}\alpha\\ \dot{\alpha}\end{bmatrix};\quad \mathbf{M}=\begin{bmatrix}0 & 1\\ -\Omega'^2 & -\nu'\end{bmatrix};\quad \mathbf{F}=-s\begin{bmatrix}0\\ \overline{q}_0(t)\overline{r}_0(t)\end{bmatrix};\\ \nu'=\frac{\nu I_{cx}}{I_{2x}I_{1x}}>0;\quad \Omega'^2=\frac{\chi I_{cx}}{I_{2x}I_{1x}}>0;\quad s=\frac{kI_{cx}}{I_{2x}I_{1x}}.\end{gathered} \tag{41}$$

The formal analytical solution of the system (40) for $\left\{\alpha(t),\dot{\alpha}(t)\right\}$ is:

$$\boldsymbol{\varphi}(t)=\boldsymbol{\Phi}(t)\cdot\boldsymbol{\Phi}^{-1}(0)\cdot\begin{bmatrix}\alpha(0)\\ \dot{\alpha}(0)\end{bmatrix}+\boldsymbol{\Phi}(t)\cdot\int_0^t\boldsymbol{\Phi}^{-1}(\xi)\cdot\mathbf{F}(\xi)d\xi; \tag{42}$$

where the following fundamental matrix is used:

$$\begin{gathered}\boldsymbol{\Phi}(t)=\begin{bmatrix}e^{\lambda_1 t} & e^{\lambda_2 t}\\ \lambda_1 e^{\lambda_1 t} & \lambda_2 e^{\lambda_2 t}\end{bmatrix};\quad \boldsymbol{\Phi}^{-1}(t)=\frac{1}{(\lambda_2-\lambda_1)}\begin{bmatrix}\lambda_2/e^{\lambda_1 t} & -1/e^{\lambda_1 t}\\ -\lambda_1/e^{\lambda_2 t} & 1/e^{\lambda_2 t}\end{bmatrix};\\ \lambda_{1,2}=\frac{1}{2}\left(-\nu'\pm\sqrt{\nu'^2-4\Omega'^2}\right)\in\mathbb{C}.\end{gathered} \tag{43}$$

It case of the small oscillations, we can assume that the initial values are:

$$\alpha(0)=\mu_{\alpha}<<1;\quad \dot{\alpha}(0)=0. \tag{44}$$

6.2. The analytical scheme of the Melnikov method adaptation

Basing on the first component of solution (42) we can write the integrand (30):

$$\left[f_L g_l - f_l g_L \right]\Big|_{\left(\bar{L}(t),\bar{l}(t),t+t_0\right)} = \varphi_1(t+t_0)\, f\left(\bar{p}_0(t),\bar{q}_0(t),\bar{r}_0(t)\right), \tag{45}$$

$$\varphi_1(t+t_0) = \frac{e^{\lambda_1(t+t_0)}}{(\lambda_2-\lambda_1)}\left(\mu_\alpha\lambda_2 + s\int_0^{t+t_0}\frac{\bar{q}_0(\xi)\bar{r}_0(\xi)}{e^{\lambda_1\xi}}d\xi\right) + \\ + \frac{e^{\lambda_2(t+t_0)}}{(\lambda_2-\lambda_1)}\left(-\mu_\alpha\lambda_1 - s\int_0^{t+t_0}\frac{\bar{q}_0(\xi)\bar{r}_0(\xi)}{e^{\lambda_2\xi}}d\xi\right). \tag{46}$$

The expression (46) represents the rewritten form of analytical solution for the angle $\bar{\alpha}(t+t_0)$ strictly along the heteroclinic separatrix. The expression (46) corresponds to the real function, regardless of complex conjugate values $\lambda_{1,2}$ (43).

In the framework of presented adaptation we can change the integration variable in the Melnikov integral (26):

$$\tau = t + t_0. \tag{47}$$

Let us remind, that t (and τ) – is the usual physical time of the dynamical process; and t_0 – is the "sliding parameter", which describes local positions along the unperturbed separatrix. The parameter t_0 also defines the t_0–parametric family of the heteroclinic solutions shifted relative to each other along the physical time axis. In other words, the parameter t_0 shifts the starting point along the heteroclinic separatrix and changes the initial conditions of the motion. After changing the variable (47), the Melnikov integral (26) can be rewritten in the equivalent form:

$$M(t_0) = \int_{-\infty}^{+\infty}\left[f_L g_l - f_l g_L \right]\Big|_{\left(\bar{L}(\tau-t_0),\bar{l}(\tau-t_0),\tau\right)} d\tau, \tag{48}$$

where the specific shape of the integrand is:

$$\left[f_L g_l - f_l g_L \right]\Big|_{\left(\bar{L}(\tau-t_0),\bar{l}(\tau-t_0),\tau\right)} = \varphi_1(\tau)\cdot f\left(\bar{p}_0(\tau-t_0),\bar{q}_0(\tau-t_0),\bar{r}_0(\tau-t_0)\right). \tag{49}$$

As we see from (49), the sliding parameter t_0 now "shifts" along the τ-axis the graph of the factor $f(\tau-t_0)$, which is analytically defined by the expression (31). The factor $\varphi_1(\tau)$ corresponds to the time-dependence of the small perturbation (in the present case it is a small angle $\alpha(\tau)$).

Here we should give some comments on the improper integration during the calculation of the Melnikov integral in the form (48) with the integrand (49).

1) The Melnikov integral (48) as an improper integral can not converge when the perturbation $\varphi_1(\tau)$ is unbounded, and can converge to its bounded value in such cases when the function $f(\tau)$ is converging to zero at $\tau \to \pm\infty$, and when the perturbation $\varphi_1(\tau)$ is bounded (and, moreover, small) on the whole interval $\tau \in (-\infty, +\infty)$.

2) If the Melnikov integral (48) is converging and the function $f(\tau)$ is an even function converging monotonically to zero (fig.5-a) at $\tau \to \pm\infty$, then it is possible to select the closed interval $\tau \in \left[-\tau_{\text{conv}}, \tau_{\text{conv}}\right]$ as an integration interval to calculate the value of the integral (48) with any high predefined accuracy at any bounded function $\varphi_1(\tau)$.

Firstly, let us show the convergence of the improper integral (48) in cases when the bounded even function $f(\tau)$ is converging exponentially fast and monotonically to zero at $\tau \to \pm\infty$ and when the function $\varphi_1(\tau)$ is bounded.

▼

1. If the function $\varphi_1(\tau)$ is bounded, then

$\forall \tau \in (-\infty, +\infty)$: $\left|\varphi_1(\tau)\right| < \varphi_{\text{sup}} = \text{const} \ll \infty$.

2. If we have the bounded even function $f(\tau)$ converging exponentially fast and monotonically to zero at $\tau \to \pm\infty$, then the signed area $|f(\tau)|$ will be equal to some constant:

$$I^+ = \int_{-\infty}^{+\infty} \left| f(\tau) \right| d\tau = S^+ = \text{const}.$$

It is easy to understand from the convergence property of the improper integral I_R with a lower rate $R>0$ of exponential convergence (in comparison with the rate of exponential convergence of the even function $f(\tau)$ at $\tau \to \pm\infty$):

$$\forall\ our\ f(\tau) \quad \exists R = \text{const} > 0: \quad I^+ < 2I_R, \text{ where } I_R = \left| f(0) \right| \int_0^{+\infty} e^{-Rt} dt = \frac{\left| f(0) \right|}{R}.$$

This means the absolute convergence of the integral I^+.

3. From the absolute convergence of I^+ the convergence of the improper integral (48) follows:

$$\forall t_0: \quad S^+ \varphi_{\text{sup}} > \int_{-\infty}^{+\infty} \left| f(\xi) \varphi_1(\xi + t_0) \right| d(\xi + t_0) > \int_{-\infty}^{+\infty} f(\tau - t_0) \varphi_1(\tau) d\tau,$$

therefore, the improper integral (48) is converging.

▲

Secondly, let us define the parameter τ_{conv} more accurately:

▼

As we have already shown, the integral (48) is converging at any t_0. Therefore, we can calculate this integral by numerical methods with any predefined accuracy for any arbitrary value t_0. Moreover, in the framework of the numerical calculation with the predefined accuracy δ, we can detect the appropriate bound of numerical integration $\left[\overline{t}_0 - \tau_\delta, \overline{t}_0 + \tau_\delta\right]$ at calculations for the specific value $\overline{t}_0$:

$$M(\overline{t}_0) = \int_{-\infty}^{+\infty} f(\tau - \overline{t}_0) \varphi_1(\tau) d\tau \underset{\delta}{\cong} \int_{\overline{t}_0 - \tau_\delta}^{\overline{t}_0 + \tau_\delta} f(\tau - \overline{t}_0) \varphi_1(\tau) d\tau. \qquad (50)$$

Choosing an interval of interest $\overline{t}_0 \in \left[t_0^{begin}, t_0^{end}\right]$, we can find the largest

integration bounds $\tau_{\delta}^{\sup}$ to guarantee the accuracy δ for the integral value on the whole interval $t_0 \in \left[t_0^{begin}, t_0^{end}\right]$. So, we can define this value as an integration bound τ_{conv} which guarantee the predefined accuracy δ of the improper integral (48) calculation:

$$\forall \delta \ \ and \ \ \forall t_0 \in \left[t_0^{begin}, t_0^{end}\right] \ \exists \tau_{conv}: \\ \left| \int_{t_0-\tau_{conv}}^{t_0+\tau_{conv}} f\left(\tau - t_0\right)\varphi_1\left(\tau\right)d\tau - \bar{I}\left(t_0\right) \right| \le \delta, \tag{51}$$

where $\bar{I}\left(t_0\right)$ is the exact value of the integral (48).

▲

With the above explanations fulfilled we can make the following third comment.

3) The graph of the integrand (49) depends on the sliding parameter t_0, but it has a bounded shape (the blue curve at fig.5-b, -d) converging to zero on the closed interval $\tau \in \left[t_0 - \tau_{\text{conv}}, t_0 + \tau_{\text{conv}}\right]$. Moreover, the signed area bounded by (49) on the interval $\tau \in \left[t_0 - \tau_{\text{conv}}, t_0 + \tau_{\text{conv}}\right]$ will correspond to the value of the improper integral (48), calculated with the accuracy δ. Let us call this geometrical shape as "the Melnikov hill". This hill slides along the τ-axis and changes its own area at the change of the sliding parameter t_0 value. Values of the Melnikov function $M(t_0)$ will be equal to the Melnikov hill areas at specific values of the sliding parameter t_0 with the accuracy δ.

It is important to note here, that the Melnikov hill parametrically slides together with the sliding parameter t_0 over the "fixed" graph of the small perturbation $\varphi_1\left(\tau\right)$ (green lines in fig.5-b – d). In other words, only a limited part of the real physical perturbing time-process is essential inside the closed interval of the Melnikov hill$\left(\tau \in \left[t_0 - \tau_{\text{conv}}, t_0 + \tau_{\text{conv}}\right]\right)$: only this "local" time-interval $\left(\tau \in \left[t_0 - \tau_{\text{conv}}, t_0 + \tau_{\text{conv}}\right]\right)$ of the real physical time τ of the perturbation time-process defines the area of the Melnikov hill at any t_0.

As it follows from the solution (42), the unbounded formal amplitude growth takes place for negative values of the time (fig.6); moreover, this infinite growth can be practically "instantaneous" (in reversed negative time) for large damping values. This aspect does not allow to consider the perturbation as bounded on the whole time interval ($-\infty < t < +\infty$), and, therefore, the Melnikov integral will not converge. However, it cannot be realized physically: the real dynamics arises for the zero value of the physical time (at the specific initial conditions), and further this process is carried out in the positive direction of time ($t \to +\infty$).

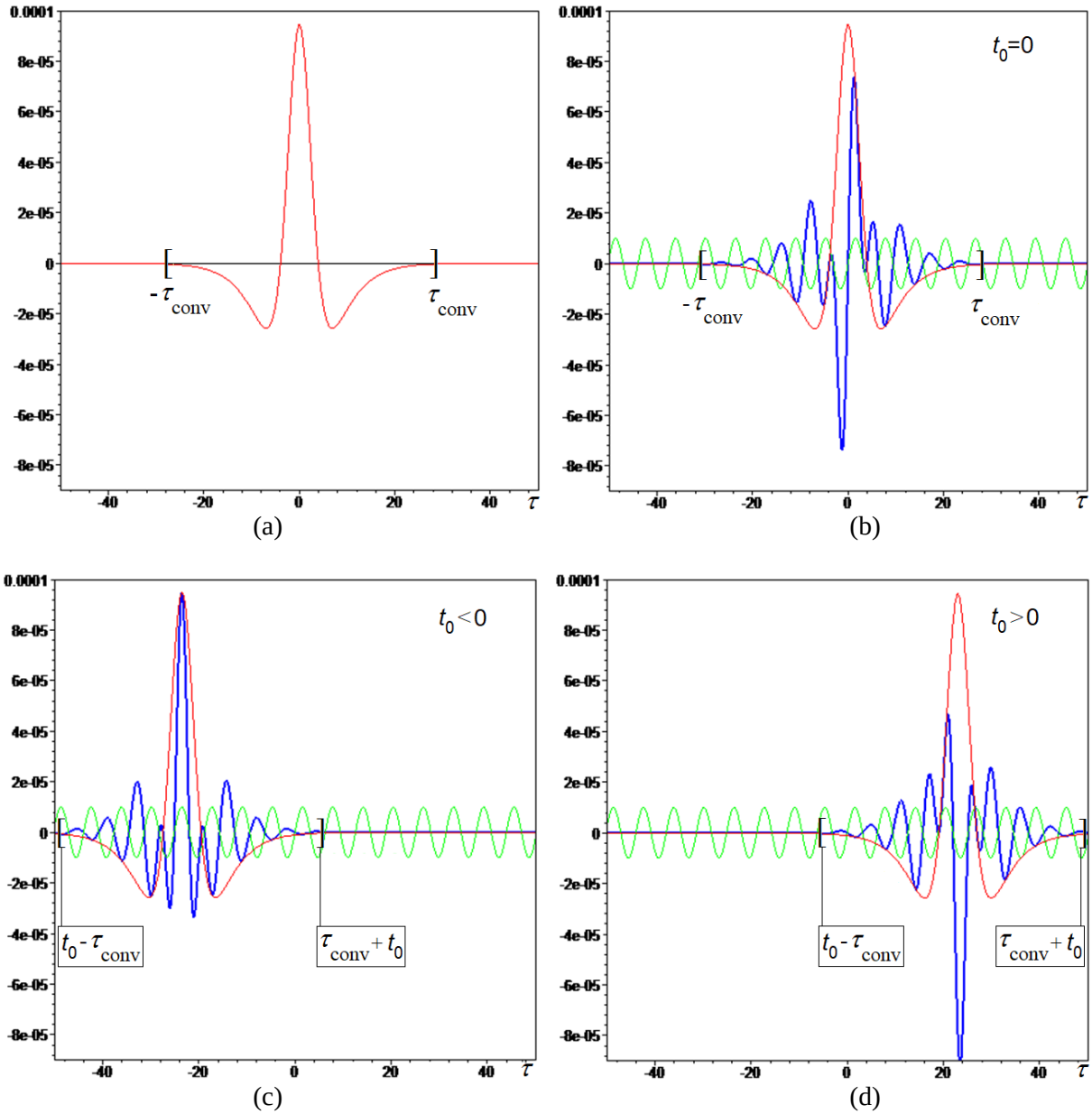

Figure 5 – The Melnikov "hill" slide:
$f(\tau\text{-}t_0)$ – red; $\varphi_1(\tau)$ – green; the Melnikov "hill" – blue

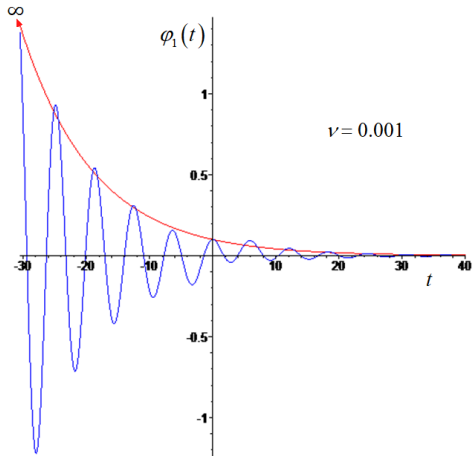

Figure 6 – The unlimited formal amplitude (42) growth
of perturbations for negative values of time

To use the Melnikov's formalism correctly and to calculate the integral (48) we can define the following shape of the small $\alpha(t)$-angle perturbation based on the solution (42):

$$\varphi_1^+(t)=\begin{cases}\varphi_1(t),\ if\ \ t\geq 0;\\ 0,\ if\ \ t<0,\end{cases} \tag{52}$$

or, the same is

$$\varphi_1^+(t)=\mathrm{H}(t)\varphi_1(t), \tag{53}$$

where $\mathrm{H}(t)$ is the Heaviside function. The form of the small perturbation (53) describes the natural physical perturbation time-process, that absents before its own start (at $t<0$). The time-dependence $\varphi_1^+(t)$ has different forms (fig.7) for various values of damping v.

In the first limiting case at $v = 0$, the dependence $\varphi_1^+(t)$ have a tendency to pure harmonic oscillations. In the second limiting case at $v = \infty$ the dependence $\varphi_1^+(t)$ keeps its initial value constant (that can be expressed with the help of the Heaviside function):

$$\bar{\varphi}_1^+(t)=\mu_\alpha \mathrm{H}(t). \tag{54}$$

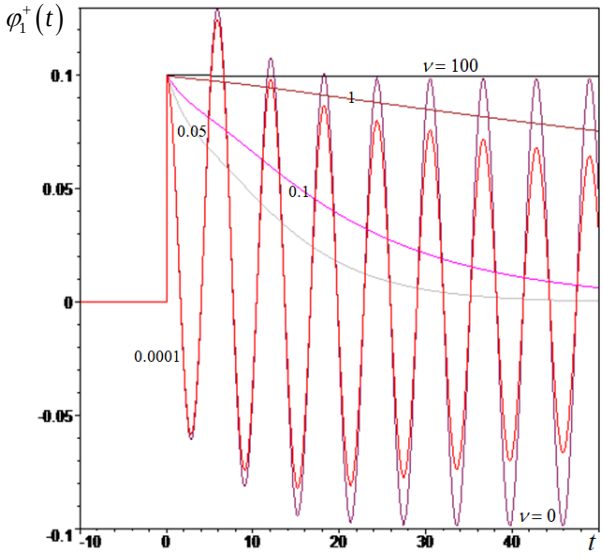

Figure 7 – The $\varphi_1^+(t)$ at different values of damping $v\left[\mathrm{kg}\times\mathrm{m}^2/\mathrm{s}\right]$

Let us calculate the Melnikov integral (48) in the case of the infinitely large damping ($v=\infty$) with the corresponded perturbation (54):

$$M(t_0)=\int_{-\infty}^{+\infty}\left[f_L g_l-f_l g_L\right]\Big|_{\left(\bar{L}(\tau-t_0),\bar{l}(\tau-t_0),\tau\right)}d\tau=$$
$$=\int_{-\infty}^{+\infty}\mu_\alpha \mathrm{H}(\tau)\,f(\tau-t_0)\,d\tau=\mu_\alpha\int_{0}^{+\infty}f(\tau-t_0)\,d\tau=\mu_\alpha\int_{-t_0}^{+\infty}f(\xi)\,d\xi. \tag{55}$$

For the purpose of analytical integration of the integral (55), we can rewrite function $f(t)$ using expressions (29):

$$f(t)=\frac{f_L g_l - f_l g_L}{\tilde{\alpha}(t+t_0)}=\frac{k}{I_{cy}I_{cz}\left(G^2-I_{cz}^2\bar{r}_0^{\,2}\right)}\Bigg(\bar{p}_0^{\,3}\bar{r}_0^{\,2}I_{cx}^2I_{cz}^2+\bar{q}_0^{\,2}\bar{r}_0^{\,2}\bar{p}_0I_{cy}I_{cz}^2I_{cx}-$$
$$-\bar{r}_0^{\,2}\left(G^2-I_{cz}^2\bar{r}_0^{\,2}\right)\bar{p}_0I_{cz}I_{cx}+G^2\bar{q}_0^{\,2}\bar{p}_0I_{cy}\left(I_{cx}-I_{cy}\right)-2\bar{r}_0^{\,2}\bar{q}_0^{\,2}\bar{p}_0I_{cz}^2I_{cy}\left(I_{cx}-I_{cy}\right)\Bigg). \tag{56}$$

Here it is possible to remind the following expressions for the angular momentum components of a rigid body (that also will be true for the heteroclinic case as well):

$$\begin{cases} K_x=I_{cx}\bar{p}_0;\ \ K_y=I_{cy}\bar{q}_0;\ \ K_z=I_{cz}\bar{r}_0\ ; \\ G^2-I_{cz}^2\bar{r}_0^{\,2}=K_x^2+K_y^2; \\ \dot{K}_x=\left(I_{cy}-I_{cz}\right)\bar{q}_0\bar{r}_0\ ;\ \dot{K}_y=\left(I_{cz}-I_{cx}\right)\bar{r}_0\bar{p}_0;\ \ \dot{K}_z=\left(I_{cx}-I_{cy}\right)\bar{p}_0\bar{q}_0\,. \end{cases} \tag{57}$$

With the help of (57) we can simplify (56):

$$\begin{aligned} f(t)&=\frac{k}{I_{cy}I_{cz}}\left(\bar{p}_0\left(K_z^2-K_y^2\right)+\bar{q}_0K_xK_y-\bar{r}_0K_zK_x\right)= \\ &=\frac{k}{I_{cy}I_{cz}}\left(K_y\left(\bar{q}_0K_x-\bar{p}_0K_y\right)+K_z\left(\bar{p}_0K_z-\bar{r}_0K_x\right)\right)= \\ &=\frac{k}{I_{cy}I_{cz}}\left(K_y\bar{p}_0\bar{q}_0\left(I_{cx}-I_{cy}\right)+K_z\bar{p}_0\bar{r}_0\left(I_{cz}-I_{cx}\right)\right)= \\ &=\frac{k}{I_{cy}I_{cz}}\left(K_y\dot{K}_z+K_z\dot{K}_y\right)=\frac{k}{I_{cy}I_{cz}}\frac{d}{dt}\left(K_yK_z\right)=k\frac{d}{dt}\left(\bar{q}_0(t)\bar{r}_0(t)\right). \end{aligned} \tag{58}$$

Now the analytical value of the integral (55) follows:

$$\begin{aligned} M(t_0)&=\mu_\alpha\int_{-t_0}^{+\infty}k\frac{d}{d\xi}\left(\bar{q}_0(\xi)\bar{r}_0(\xi)\right)d\xi= \\ &=\mu_\alpha k\bar{q}_0(\xi)\bar{r}_0(\xi)\Big|_{-t_0}^{+\infty}=-\mu_\alpha k\bar{q}_0(-t_0)\bar{r}_0(-t_0). \end{aligned} \tag{59}$$

From (58) we also can find analytically the signed area S_f bounded by $f(t)$. It is exactly equal to zero[1]:

$$S_f=\int_{-\infty}^{+\infty}f(\xi)\,d\xi=k\bar{q}_0(\xi)\bar{r}_0(\xi)\Big|_{-\infty}^{+\infty}=0\,. \tag{60}$$

The numerical values of the Melnikov integral (55) and analytical calculations (59) are presented in figure (fig.8). This result is fully expected and analytically verified. The shape of $f(t)$ with the zero-value of its area (60) does not depend on specific parameters of the system – it is fully defined by the invariant heteroclinic properties of the unperturbed rigid body dynamics.

As we see from the results for the Melnikov integral (55), in the case of infinitely large damping (under the piecewise perturbation (54)), the simple zero

[1] Also from the fact $S_f = 0$, we can conclude, that the blue area under the $f(t)$ curve (fig.3) is exactly equal to the finite red area. Then, moreover, it is obvious that the absolute area I^+ will be exactly equal to twice the value of the red area, i.e. I^+=const and, therefore, the improper integral (48) is converging.

takes place at t_0=0. At the same time, it is obvious that the case of the motion for the infinitely large damping value is fully regular, because all perturbing oscillations here are completely eliminated. This is a prime example of the possible existence of several Melnikov's integral zeros, which arise formally in known regular cases as zero-areas of Melnikov hills only due to the geometrical properties of the curve $f(\tau)$ and the piecewise perturbing factor (52). Such formal zeros can also be possible in other cases for piecewise functions of perturbations (52). So, let us call such formal zeros of the Melnikov hills/functions as the "*fictive zero*s". We should ignore such fictive zeros in analysis of roots in the modified Melnikov method. In the task of the nanosatellite with movable unit we have only one fictive zero (fig.8).

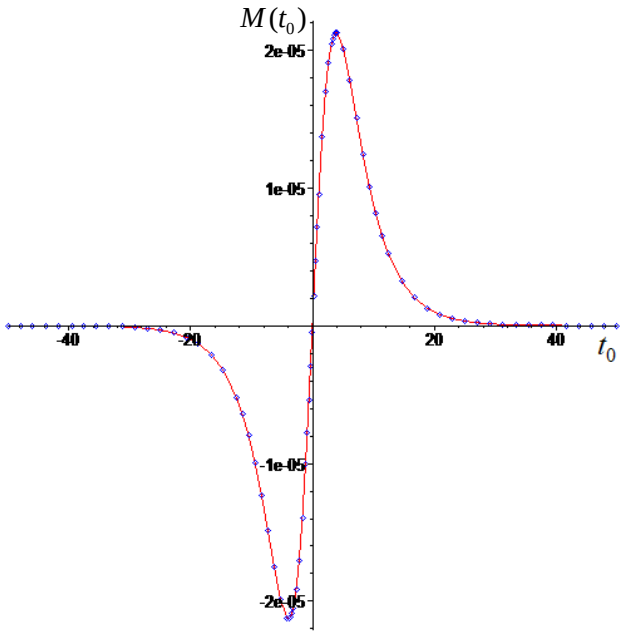

Figure 8 – The single fictive zero of the Melnikov integral (55) for the extremely large damping value (v = 100):
red line – numerical calculations of (55); blue dots – analytical values (59)

At the decrease of the damping value, the form of perturbations (52) will change (fig.7); and we will detect the appearance of new simple roots of the integral (48) besides the fictive zeros. Exactly this appearance of such new roots will indicate the birth of the heteroclinic chaos in the dynamics. Therefore, these new zeros can be called as the "*substantial zeros*". We should note that in fact, all of the infinite quantity of substantial roots arise immediately with the first one, but they can be invisible in the current tolerance scale, and they become quite visible when the damping will be reduced.

So, to detect the chaos with help of the adapted Melnikov formalism, we have to detect the substantial zeros of the integral (48) with piecewise functions of perturbations (52):

$$M(t_0) = \int_{-\infty}^{+\infty} \varphi_1^+(\tau)\, f(\tau - t_0)\, d\tau \cong \int_{t_0-\tau_{\text{conv}}}^{t_0+\tau_{\text{conv}}} \varphi_1^+(\tau)\, f(\tau - t_0)\, d\tau\,. \qquad (61)$$

6.3. The numerical evaluation of the chaotic dynamics properties

We cannot analytically integrate the integral (61) in quadratures for arbitrary values of the damping. For this reason, we will conduct the numerical calculation for different values of damping with parameters from the table 1.

First of all, it is possible to present the numerical results for the Melnikov functions (61), which are presented in fig.9. Figure (fig.9) shows the gradual deformation of the Melnikov function forms starting from the regular case (fig.9-a, upper detailed part of the figure) for the large damping value (ν = 55), and finishing with the obvious chaotic dynamics (Fig.9-f) for the small damping value (ν = 0.0001). This gradual deformation shows that the first substantial zero appears around ν < 35 (fig.9-a, the lower detailed part of the figure). The infinite set of substantial zeros becomes clearly visible at ν = 0.001 (fig.9-e). As we have already mentioned, the first substantial zero can be detected at ν = 35 [kg·m^2/s] – this value can be considered as the parametric boundary for the occurrence of the heteroclinic chaos.

The detected boundary value of the damping can be confirmed by the Poincaré sections (fig. 10). The Poincaré sections are plotted, as previously, in the phase space (l, L/G) by the "stroboscopic" condition $\left(\mathrm{mod}\left[t, 2\pi/\bar{\Omega}\right] = 0\right)$ with the "basic frequency" $\bar{\Omega} = \mathrm{Im}\left(\lambda_{1,2}\right)$ in accordance with (43); or when Im(λ) = 0, this frequency is equal to the natural frequency $\bar{\Omega} = \Omega'$ of torque-free oscillations (41).

It is worth to note some aspects following from numerical results. With an extremely large damping value the phase portrait and Poincaré section will have a typical unperturbed regular form (fig.4-b). For the boundary damping value the chaotic layer appears near separatrices (red points at fig.10-a). In case of the further damping decreasing, the chaotic layer develops and expands (fig.10-b – f).

At the end of numerical confirmations we present the comparative calculation (fig.11) of the two forms of the Melnikov functions for the damping absence (ν = 0). The first variant corresponds to the classical Melnikov method with the function (35) at $\mu = \mu_\alpha = \alpha(0) = 0.1$; $\Omega = \bar{\Omega} = \mathbf{w} = 1.022$ [1/s], when the amplitude of the function (36) is equal to $\Lambda = 0.4208 \cdot 10^{-5}$ [kg·m^2/s^2]. In the second variant, the adapted Melnikov method was used and the function (61) was calculated for the same initial values.

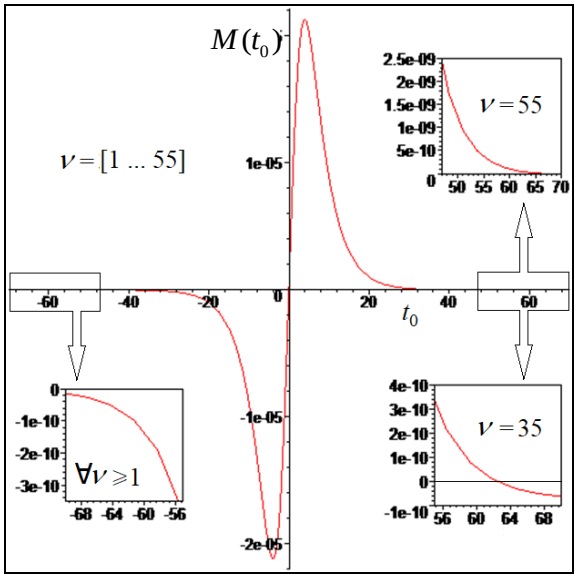

(a)

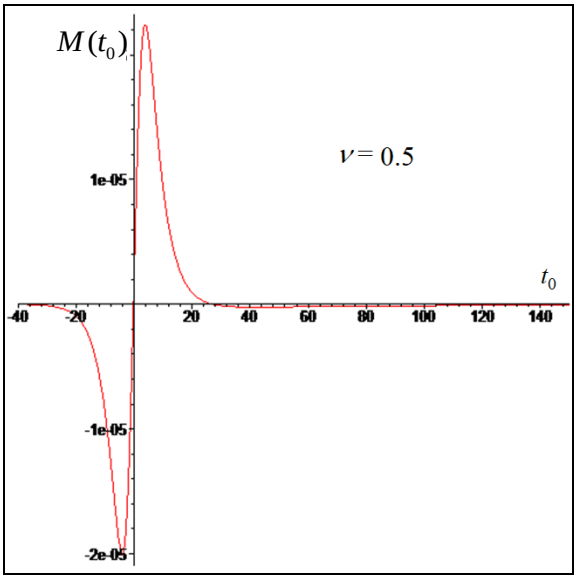

(b)

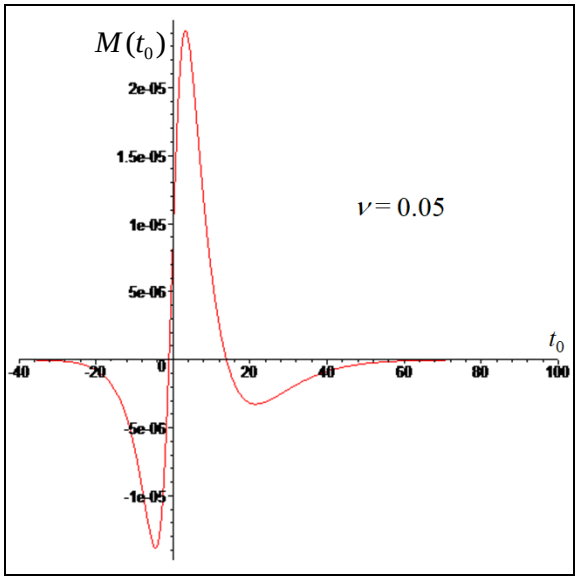

(c)

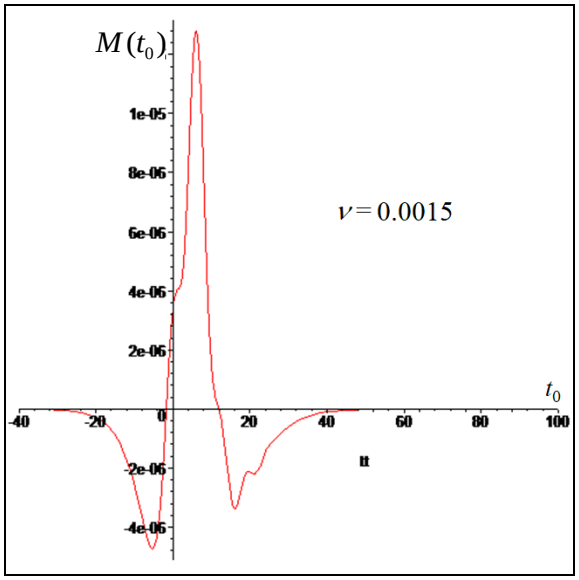

(d)

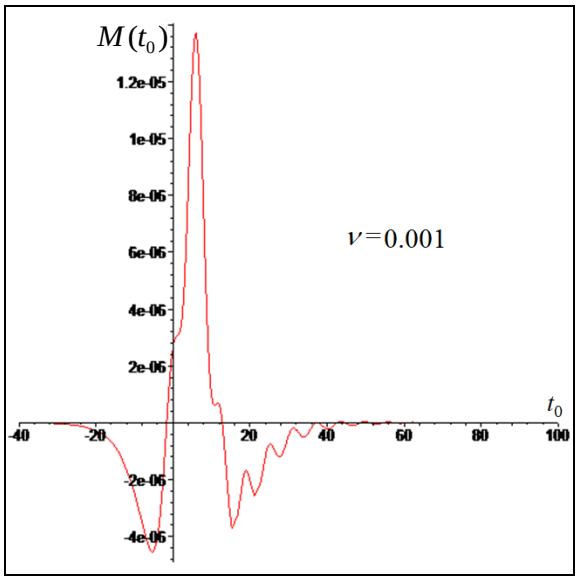

(e)

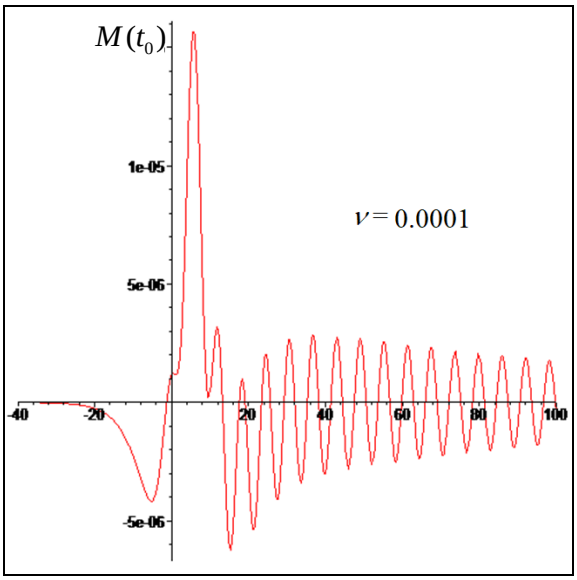

(f)

Figure 9 – The Melnikov functions at different values ν [kg·m^2/s]

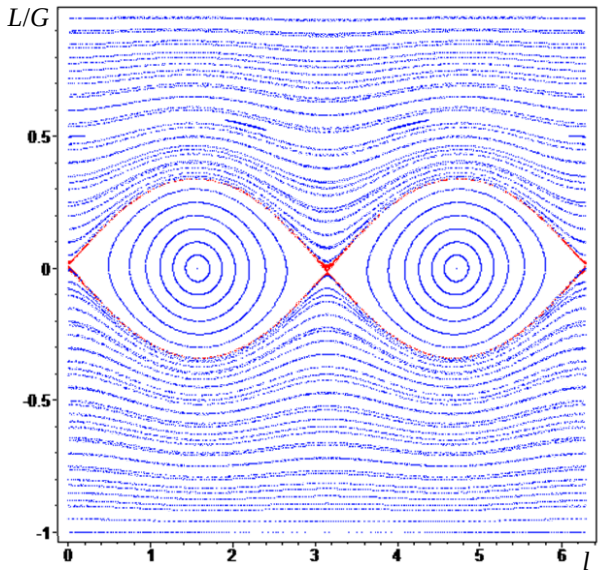

(a): ν=35; $\bar{\Omega}$=1.044

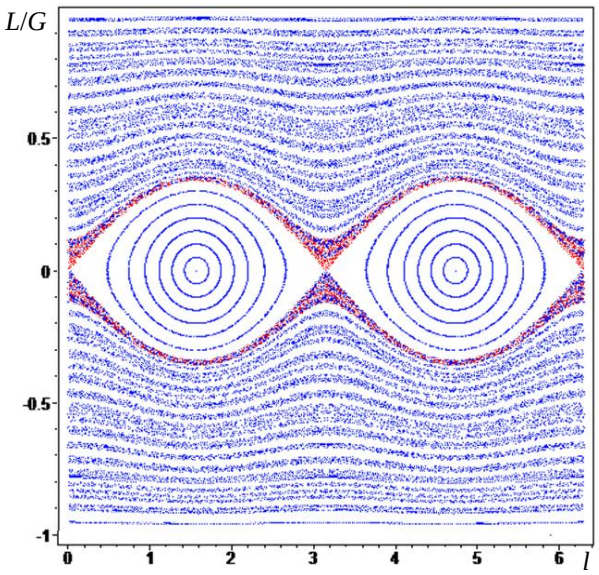

(b): ν=5; $\bar{\Omega}$=1.044

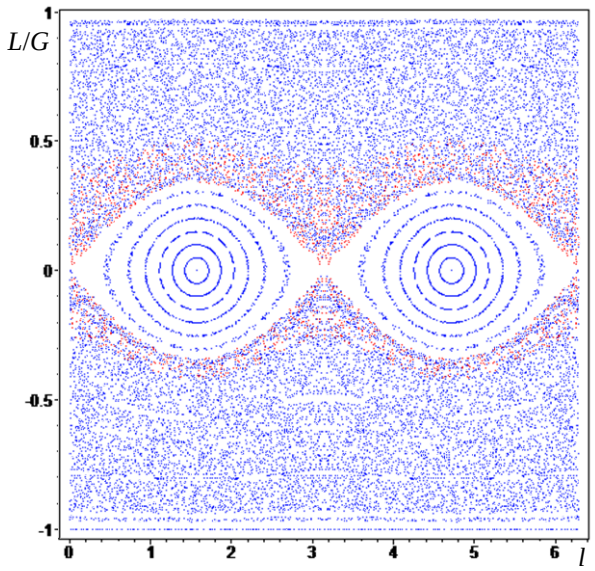

(c): ν=0.5; $\bar{\Omega}$=1.044

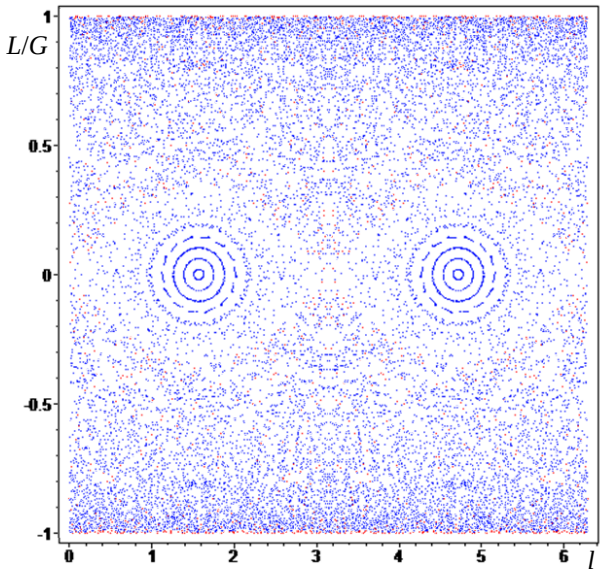

(d): ν=0.05; $\bar{\Omega}$=1.044

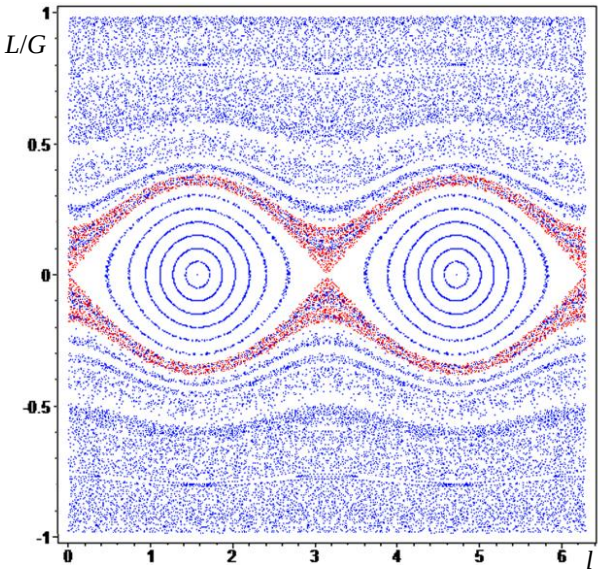

(e): ν=0.0001; $\bar{\Omega}$=1.021

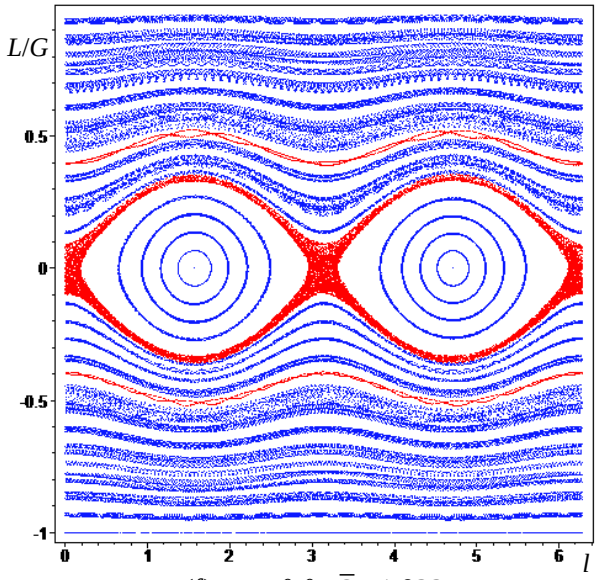

(f): ν=0.0; $\bar{\Omega}$=1.022

Figure 10 - Poincaré sections

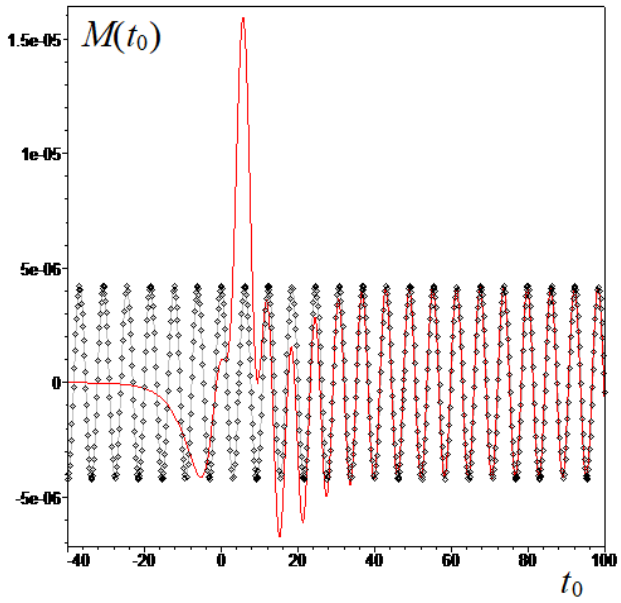

Figure 11 – The comparative calculation
of the two cases of the Melnikov functions $M(t_0)$ at $v = 0$:
the expression (61) – red line; the expression (35) – black dots on grey line

Thus, based on numerical results, it is possible to finally confirm the workability of the presented adaptation of the Melnikov method for evaluating the parametric boundary of the heteroclinic chaos occurrence.

Conclusion

In the present paper, the problem of the heteroclinic chaos detecting in dynamical systems with damped perturbations was considered on the basis of the Melnikov method adaptation.

The first advantage of the method adaptation is its workability in the cases of the perturbations amplitudes decrease. The adapted approach allows to ignore the formal infinite exponential growth of the perturbation amplitude in the reverse direction of time, when the classical method is inapplicable due to the non-convergence of the improper Melnikov integrals.

The second advantage of the developed approach is the transparent geometric interpretation of the value of the Melnikov function as an area of the Melnikov hill plotted for the specific point of the parametric time. The idea of the Melnikov hill allows to use only local closed interval of the physical time around the specific moment of the parametrical time in the framework of the Melnikov integral calculation.

With the help of the adapted Melnikov method, the chaotic dynamics of a nanosatellite with a slightly movable unit was investigated. The corresponding

critical “boundary damping values” were found in the case of damped perturbing oscillations of the movable unit.

Acknowledgments

This work is supported by the Russian Science Foundation (# 19-19-00085).

CRediT authorship contribution statement

Anton V. Doroshin: Conceptualization, Methodology, Formal analysis, Funding acquisition, Investigation, Supervision, Writing – original draft, Writing – review & editing, the Melnikov method adaptation (the section #6), the natural perturbation case investigation (the section #6).

Alexander V. Eryomenko: Formal analysis, Investigation, Software, Validation, Visualization, Writing – original draft, Writing – rewiew & editing, Mathematical models of the nanosatellite with one movable unit (the sections #2, 3), the harmonic perturbation case investigation (the section #5).

Declaration of competing interest

We can declare that the authors have not known competing financial interests or personal relationships that could appear to influence this research publishing.

References

[1] Akulenko, L. D., Kozachenko, T. A., & Leshchenko, D. D. (2019). Time quasi-optimal deceleration of rotations of a gyrostat with a moving mass in a resistive medium. Journal of Computer and Systems Sciences International, 58(5), 667-673.

[2] Andoyer H. (1923), Cours de Mecanique Celeste, Paris: Gauthier-Villars.

[3] Arnold V.I. (1964). Instability of dynamical systems with several degrees of freedom, Doklady Akademii Nauk SSSR, 156 (1), pp. 9-12.

[4] Arnold, V.I. (1963). Proof of AN Kolmogorov’s theorem on the conservation of conditionally periodic motions with a small variation in the Hamiltonian. Russian Math. Surv, 18(9).

[5] Aslanov V. S., Doroshin A. V., Eremenko A. V. (2019) Attitude dynamics of nanosatellite with a module on retractable beams, J. Phys.: Conf. Ser. 1260 (2019), 112004.

[6] Aslanov, V. S. (2015). Chaotic behavior of a body in a resistant medium. International Journal of Non-Linear Mechanics, 73, 85-93.

[7] Aslanov, V.S. (2017). Rigid body dynamics for space applications. Butterworth-Heinemann.

[8] Aslanov, V.S. (2021). Chaotic attitude dynamics of a LEO satellite with flexible panels. Acta Astronautica, 180, 538-544.

[9] Aslanov, V.S., & Doroshin, A.V. (2010). Chaotic dynamics of an unbalanced gyrostat. Journal of Applied Mathematics and Mechanics, Volume 74, Issue 5, pp.525-535.

[10] Aslanov, V.S., & Sizov, D.A. (2021). Chaos in flexible CubeSat attitude motion due to aerodynamic instability. Acta Astronautica, 189, 310-320.

[11] Aslanov, V.S., Doroshin, A.V., & Eremenko, A.V. (2019). Attitude dynamics of nanosatellite with a module on retractable beams. In Journal of Physics: Conference Series (Vol. 1260, No. 11, p. 112004). IOP Publishing.
[12] Bandyopadhyay, S., Foust, R., Subramanian, G. P., Chung, S. J., & Hadaegh, F. Y. (2016) Review of formation flying and constellation missions using nanosatellites. Journal of Spacecraft and Rockets, 53(3), 567-578.
[13] Bao-Zeng, Y. (2011). Study on the Chaotic Dynamics in Attitude Maneuver of Liquid-Filled Flexible Spacecraft, AIAA Journal, Vol. 49, No. 10, pp. 2090-2099.
[14] Beletskiĭ, V.V., Pivovarov, M.L., & Starostin, E.L. (1996). Regular and chaotic motions in applied dynamics of a rigid body. Chaos: An Interdisciplinary Journal of Nonlinear Science, 6(2), 155-166.
[15] Beletsky V.V. (1995), Reguläre und chaotische Bewegung starrer Körper. Teubner.
[16] Belokonov, I. V., Timbai, I. A., & Nikolaev, P. N. (2018). Analysis and Synthesis of Motion of Aerodynamically Stabilized Nanosatellites of the CubeSat Design. Gyroscopy and Navigation, 9(4), 287-300.
[17] Blackwell, W., Pereira, J. (2015) New Small Satellite Capabilities for Microwave Atmospheric Remote Sensing: The Earth Observing Nanosatellite-Microwave (EON-MW) MIT Lincoln Laboratory (http://digitalcommons.usu.edu/cgi/viewcontent.cgi?article=3292&context=smallsat)
[18] Boccaletti, S., Grebogi, C., Lai, Y. C., Mancini, H., & Maza, D. (2000). The control of chaos: theory and applications. Physics reports, 329(3), pp. 103-197.
[19] Chen Li-Qun, Liu Yan-Zhu (2002). Chaotic attitude motion of a magnetic rigid spacecraft and its control, International Journal of Non-Linear Mechanics 37, pp. 493–504.
[20] Chernousko, F. L., Akulenko, L. D., Leshchenko, D.D. (2017) Evoluton of Motions of a Rigid Body About its Center of Mass. Cham: Springer, 2017. 241 p.
[21] Deprit A. (1967). A free rotation of a rigid body studied in the phase plane, American Journal of Physics 35, pp.424 428.
[22] Doroshin, A.V. (2012). Heteroclinic dynamics and attitude motion chaotization of coaxial bodies and dual-spin spacecraft. Communications in Nonlinear Science and Numerical Simulation, 17 (3), pp. 1460-1474.
[23] Doroshin, A. V. (2016-a). Heteroclinic chaos and its local suppression in attitude dynamics of an asymmetrical dual-spin spacecraft and gyrostat-satellites. The Part I—Main models and solutions. Communications in Nonlinear Science and Numerical Simulation, 31(1-3), 151-170.
[24] Doroshin, A. V. (2016-b). Heteroclinic Chaos and Its Local Suppression in Attitude Dynamics of an Asymmetrical Dual-Spin Spacecraft and Gyrostat-Satellites. The Part II – The heteroclinic chaos investigation, Communications in Nonlinear Science and Numerical Simulation, 31 (1-3), pp. 171-196.
[25] Doroshin, A. V. (2018). Chaos as the hub of systems dynamics. The part I—The attitude control of spacecraft by involving in the heteroclinic chaos. Communications in Nonlinear Science and Numerical Simulation, 59, 47-66.
[26] Doroshin, A. V., & Eremenko, A. V. (2019). Shilnikov's homoclinic loops in attitude dynamics of CubeSAT-3U nanosatellites with one movable unit. Lecture Notes in Engineering and Computer Science, 2239, 73-76.
[27] Doroshin, A. V., & Eremenko, A. V. (2021-a). Attitude control of nanosatellite with single thruster using relative displacements of movable unit. Proceedings of the Institution of Mechanical Engineers, Part G: Journal of Aerospace Engineering, 235(7), 758-767.
[28] Doroshin, A. V., & Eryomenko, A. V. (2021-b) Aspects of Chaotic Regimes of a Nanosatellite With Movable Unit, Lecture Notes in Engineering and Computer Science: Proceedings of The International MultiConference of Engineers and Computer Scientists 2021, 20-22 October, 2021, Hong Kong, pp39-43.
[29] Guckenheimer, J., & Holmes, P.J. (1983). Nonlinear oscillations, dynamical systems, and bifurcations of vector fields. Vol. 42. Springer Science & Business Media.

[30] Holmes, P.J. (1990). Poincaré, celestial mechanics, dynamical-systems theory and chaos – Physics Reports (Review Section of Physics Letters) 193, No. 3, pp. 137—163 (North-Holland).
[31] Holmes, P.J., & Marsden, J.E. (1983), Horseshoes and Arnold diffusion for Hamiltonian systems on Lie groups, Indiana Univ. Math. J. 32, pp. 273-309.
[32] Iñarrea, M. (2009). Chaos and its control in the pitch motion of an asymmetric magnetic spacecraft in polar elliptic orbit, Chaos, Solitons & Fractals,Volume 40, Issue 4, pp.1637-1652.
[33] Iñarrea, M., and Lanchares, V. (2000). Chaos in the reorientation process of a dual-spin spacecraft with time-dependent moments of inertia, Int. J. Bifurcation and Chaos. 10, pp. 997-1018.
[34] Iñarrea, M., Lanchares, V., Rothos, V. M., Salas, J. P. (2003). Chaotic rotations of an asymmetric body with timedependent moment of inertia and viscous drag, International Journal of Bifurcation and Chaos, Vol. 13, No. 2, pp. 393-409.
[35] Kozlov, V.V. (1980). Methods of Qualitative Analysis in the Dynamics of a Rigid Body, Gos. Univ., Moscow.
[36] Kozlov, V.V. (1983). Integrability and non-integrability in Hamiltonian mechanics. Russian Mathematical Surveys, 38(1).
[37] Kuang Jinlu, Tan Soonhie, Arichandran Kandiah, Leung A.Y.T. (2001), Chaotic dynamics of an asymmetrical gyrostat, International Journal of Non-Linear Mechanics 36, pp. 1213-1233.
[38] Kuang, J.L., Meehan, P.A., Leung, A.Y.T. (2006), On the chaotic rotation of a liquid-filled gyrostat via the Melnikov–Holmes–Marsden integral, International Journal of Non-Linear Mechanics 41, pp. 475 – 490.
[39] Liang He, Wenjie Ma, Pengyu Gao, Tao Sheng (2020). Developments of attitude determination and control system of microsats: A survey// Proccedings of the Institution of Mechanical Engineers. Part 1: Journal of Systems and Control Engineering. 2020. First published January 6, 2020. DOI 10.1177/0959651819895173. pp.1-20.
[40] Lichtenberg, A.J., and Lieberman, M.A. (1983). Regular and stochastic motion. Vol. 38. Springer Science & Business Media.
[41] Liu, Y., Chen, L. (2013). Chaos in Attitude Dynamics of Spacecraft. Springer, Berlin, Heidelberg. https://doi.org/10.1007/978-3-642-30080-6
[42] Melnikov, V.K. (1963), On the stability of the centre for time-periodic perturbations, Trans. Moscow Math. Soc. No.12, pp. 1-57.
[43] Ovchinnikov, M. Y., & Roldugin, D. S. (2019). A survey on active magnetic attitude control algorithms for small satellites. Progress in Aerospace Sciences. 2019. V.109. Article 100546.
[44] Peng, J., & Liu, Y. (2000), Chaotic motion of a gyrostat with asymmetric rotor, International Journal of Non-Linear Mechanics, Volume 35, Issue 3, pp. 431-437.
[45] Poincaré, H. (1899), Les Methodes Nouvelles de La Mécanique Celeste, Vols. 1-3 (Gauthier Villars, Paris).
[46] Serret, J. A. (1866), Mémoire sur l'emploi de la méthode de la variation des arbitraires dans la théorie des mouvements de rotation. Mémoires de l'Academie des Sciences de Paris, Vol. 55, pp. 585-616.
[47] Tabor, M. (1989). Chaos and integrability in nonlinear dynamics. Wiley.
[48] Wiggins, S. (1988), Global Bifurcations and Chaos: Analytical Methods (Applied mathematical sciences: vol. 73). Springer-Verlag.
[49] Wiggins, S. (2003). Introduction to applied nonlinear dynamical systems and chaos. Vol. 2. Springer Science & Business Media.
[50] Ziglin S. L. (1980). Splitting of Separatrices, Branching of Solutions and Nonexistence of an Integral in the Dynamics of a Solid Body, Trans. Moscow Math. Soc. 41 (1980), pp. 287-303, transl. 1 (1982), pp. 283-298.